AD NUMBER

AD856255

LIMITATION CHANGES

TO:

Approved for public release; distribution is unlimited.

FROM:

**Distribution authorized to U.S. Gov't. agencies and their contractors;
Administrative/Operational Use; JUN 1969. Other requests shall be referred to Army Aviation Materiel Labs., Fort Eustis, VA.**

AUTHORITY

USAAMRDL ltr 23 Jun 1971

AD

USAAVLABS TECHNICAL REPORT 69-42

FLAW POINT AND DYNAMIC MICROPHOTOELASTICITY INVESTIGATION

By

A. A. Caputo

J. E. Hilzinger

June 1969

U. S. ARMY AVIATION MATERIEL LABORATORIES
FORT EUSTIS, VIRGINIA

CONTRACT DAAJ02-68-C-0023

ROCKETDYNE
A DIVISION OF NORTH AMERICAN ROCKWELL CORPORATION
CANOGA PARK, CALIFORNIA

67

DISCLAIMERS

The findings in this report are not to be construed as an official Department of the Army position unless so designated by other authorized documents.

When Government drawings, specifications, or other data are used for any purpose other than in connection with a definitely related Government procurement operation, the United States Government thereby incurs no responsibility nor any obligation whatsoever; and the fact the Government may have formulated, furnished, or in any way supplied the said drawings, specifications, or other data is not to be regarded by implication or otherwise as in any manner licensing the holder or any other person or corporation, or conveying any rights or permission, to manufacture, use, or sell any patented invention that may in any way be related thereto.

Trade names cited in this report do not constitute an official endorsement or approval of the use of such commercial hardware or software.

DISPOSITION INSTRUCTIONS

Destroy this report when no longer needed. Do not return it to the originator.

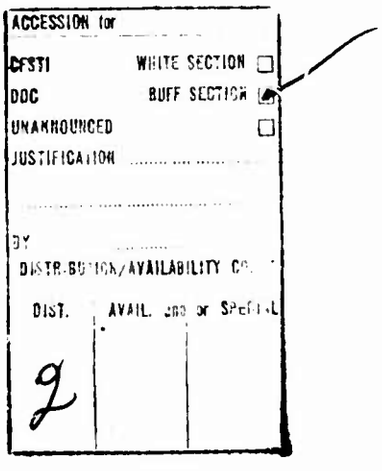

DEPARTMENT OF THE ARMY
HEADQUARTERS US ARMY AVIATION MATERIEL LABORATORIES
FORT EUSTIS, VIRGINIA 23604

This program was carried out under Contract DAAJ02-68-C-0023 with North American Rockwell Corporation, Rocketdyne Division.

The information contained in this report is a result of research conducted to extend the understanding of the behavior and response of fiber-reinforced composites when subjected to various types of loading conditions. Through experimental investigation, utilizing microphotoelastic techniques, various types of flaws related to composites were studied. In addition, the effects of using different fiber materials and fiber orientations are compared.

The report has been reviewed by the U.S. Army Aviation Materiel Laboratories and is considered to be technically sound. It is published for the exchange of information and the stimulation of future research.

Task 1F162204A17002
Contract DAAJ02-68-C-0023
USAAVLABS Technical Report 69-42
June 1969

FLAW POINT AND DYNAMIC MICROPHOTOELASTICITY INVESTIGATION

Final Report

By

A. A. Caputo and J. E. Hilzinger

Prepared by

Rocketdyne
A Division of North American Rockwell Corporation
Canoga Park, California

for
U. S. ARMY AVIATION MATERIEL LABORATORIES
FORT EUSTIS, VIRGINIA

ABSTRACT

The effects of load-induced flaws and preexisting flaws on the initiation and propagation of fracture in glass- and in graphite-fiber-reinforced composites were studied, utilizing a birefringent epoxy resin matrix with relatively wide-spaced unidirectional and simple (0° - 90° and $\pm 45^\circ$) cross-ply fiber configurations, and combining photoelastic and high-speed photographic techniques. A broad, qualitative investigation was made to characterize differences in behavior as functions of ply type and orientation, fiber identity, type of flaw (exposed edges, interior bubbles, cut filaments, and unbonded fibers), and manner of loading. Specimens were examined under simple static tension, biaxial static compression-tension and tension-tension, cyclic tension, and dynamic impact, in all cases at room temperature.

Fractures were often initiated by or drawn into the identified flaws; and fibers at angles to the principal tensile axis also constituted weak structural elements. Reduction of strength or cycle life often resulted from introduction of flaws. Fracture mode tended toward brittle in unidirectional (0°) composites and toward more complex tearing and shearing processes in other configurations and under complex loading. Formation of stacked cracks or crazing in the resin, progressive fiber unbonding, and crack bifurcation were other details observed under specific combinations of material and test parameters.

FOREWORD

The research reported herein was supported by the U.S. Army Aviation Materiel Laboratories, Fort Eustis, Virginia, under contract DAAJ02-68-C-0023 (Task 1F162204A17002), with Mr. L. T. Mazza serving as contract monitor.

The authors acknowledge the special contributions of the following individuals toward these investigations:

J. Fulton--photography and special optical assemblies.

L. A. Metcalf--test specimen preparation and assistance in performing test program.

BLANK PAGE

TABLE OF CONTENTS

LIST OF ILLUSTRATIONS

BLANK PAGE

INTRODUCTION

The mechanical behavior of composite materials is complicated by their two-phase and anisotropic nature. The strength and the detailed mechanics of fracture depend not only on the properties of the oriented constituents, but also on the interactions between them. Additional complexities occur as a result of the statistical nature of the properties of fiber bundles, of their placement in the matrix, and of the occurrence of flaws in the fiber-matrix interface or its vicinity. Effective long-range usage of advanced composites will require a basic knowledge of failure processes in these materials.

To facilitate a fundamental investigation of composite fracture and of the influence of initial flaws on fracture, a reduction of variables by modeling has been shown to be effective (Ref. 1 and 2). The present investigations employed photoelastic models consisting of 1- and 2-ply laminates with widely spaced fibers.

A broad experimental approach was taken to reveal fracture characteristics of reinforced composite materials subjected to a wide range of loading conditions. The methods developed in these investigations entailed the replacement of structural laminating resins by birefringent materials of approximately the same mechanical properties. Currently used fiber reinforcements (high-strength fiberglass and Morganite graphite fibers) were embedded in the birefringent plastic to form composite materials with low fiber concentrations but in "real" configurations, including crossplies. The resulting composites were then subjected to various uniaxial and biaxial, static and dynamic loadings of interest, while being observed photoelastically both before and during the process of fracture. Because the composite specimens are transparent and highly polished, high magnification posttest examinations of failure regions could also be performed. Further significance was given to some of the observations of fracture by the simultaneous measurements of stress and strain.

Information concerning the mechanisms of crack growth and the influence of deliberately introduced flaws, obtained from these simplified model specimens, may be used to interpret tests on structural laminates and as guidance for design analytical investigations.

MATERIAL SELECTION AND FABRICATION TECHNIQUES

MATERIAL SELECTION

Because it was intended to employ photoelastic models which are easily relatable to structural reinforced composites, actual reinforcing elements were chosen for embedment in a birefringent matrix material. High tensile strength fiberglass (HTS-901, 901 finish) was of primary interest. The rapid development of graphite fibers prompted the use of this type of fiber for comparisons, where possible, with fiberglass. Some pertinent properties of the reinforcing elements used in these investigations are presented in Table I.

TABLE I. PROPERTIES OF REINFORCING ELEMENTS

Fiber	Density, $lb/in.^3$	Modulus, $lb/in.^2 \times 10^6$	Tensile Strength, $lb/in.^2 \times 10^3$
Glass			
HTS-901	0.079	12.4	665
Morganite			
Type I	0.072	50 to 60	200 to 300
Type II	0.063	30 to 40	325 to 375

The photoelastic material used as matrix for all test specimens was a two-component epoxy system (PL-1 resin, PH-1 hardener). The cured system has mechanical properties similar to the resins used for structural composites (see below).

PL-1 PROPERTIES

A series of tests was performed to determine the mechanical and optical properties of batches of matrix to be used for reinforced specimens. Sufficient matrix was mixed for each reinforced plate casting to prepare two or three additional bars 1/2 by 1/8 by 8 inches. These specimens were polished in the same manner as described subsequently for the reinforced specimens.

Beams were subjected to four-point loading to determine stress-optical characteristics and the modulus of PL-1 plastic. Testing was performed on an Instron test machine. Beam deflection and isochromatic fringe patterns were obtained at four load levels. A typical isochromatic pattern for a four-point loaded beam is shown in Figure 1.

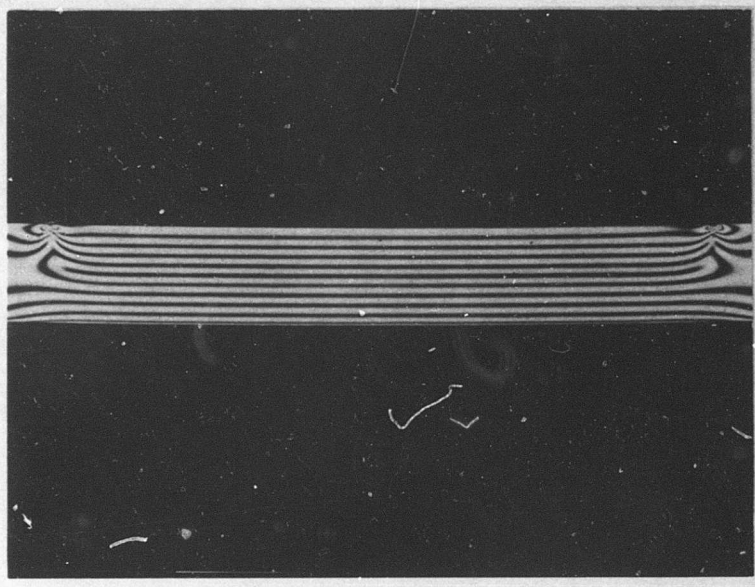

Figure 1. Isochromatic Pattern of Beam in Four-Point Loading Used for Fringe Constant Determination (1.2X).

The stress-optic law can be written as (Ref. 3)

$$\sigma_1 - \sigma_2 = \frac{fn}{t}$$

where σ_1 and σ_2 are principal stresses

f is the fringe constant

n is the fringe order

t is the model thickness

The fringe constant is the difference between principal stresses which produces a change of one order of interference in a stressed material of unit thickness. The units of f are psi per unit fringe order per inch thickness, or lb/in. order. For the four-point beam case, $\sigma_2 = 0$ and f is obtained from

$$f = \frac{\sigma_1 t}{n}$$

Modulus and fringe constant for three resin batches are summarized below:

Batch No.	E, psi	f, lb/in. order
11	618,000	120
13	605,000	125
15	620,000	109

Tensile tests were performed to determine ultimate tensile strength of PL-1. An average tensile strength (four tests) for PL-1 is 13,070 psi.

SPECIMEN FABRICATION TECHNIQUES

A special mold was designed and assembled to facilitate fabrication of unidirectional and cross-ply composite specimens. A sheet of rubber provided the casting surface. Rubber dams confined the liquid plastic to a 5- by 6-inch region. Clamping devices at the mold sides allowed for accurate placement and tensioning of reinforcing elements.

The first step of specimen fabrication consisted of placing the reinforcing elements in the clamping devices in the desired orientation. The reinforcing elements were placed over rubber dams of half the final plate thickness. After the filaments were fixed in place, a second set of rubber dams was put in position, readying the mold and the fiber network for introduction of the liquid plastic matrix material.

Each of the two matrix components (resin and hardener) was degassed in a vacuum oven to remove micro-bubbles and moisture. After degassing, the components were then combined in the appropriate proportions and carefully

mixed to avoid excessive entrapment of air. The mixture was then degassed for approximately 5 minutes and introduced into the mold, with the filaments already in place. Considerable care had to be exercised in casting the liquid plastic about the reinforcing elements so as not to trap air bubbles in the fibers or at crossover points. After casting, the reinforced plates were permitted to cure 4 days before removal from the mold.

Three types of initial flaws were introduced in some of the castings: (1) damaged fibers, (2) unbonded interfaces, and (3) matrix voids. After the fiber configuration was set in the mold clamps, some individual filaments were abraded or cut; or a short length of fiber was contaminated with mold release before the liquid matrix material was introduced. In other cases, air bubbles were introduced into the liquid plastic adjacent to a fiber by means of a hypodermic needle.

After the reinforced plates were cured, they were rough-sawed, filed, and finish-sanded to various shapes, depending on the tests to be performed, with the aid of templates. Each specimen was then carefully polished so that sharp photoelastic fringe patterns could be obtained. The specimens were roughed to the approximate desired thickness with 80-grit abrasive paper. Successively finer papers, 280 and 600 grit, were then used, followed by polishing on cloth with jeweler's rouge.

Considerable difficulty was encountered in fabricating Morganite-reinforced specimens. The Morganite fibers were supplied in the form of a tow (large bundle) containing 10,000 filaments approximately 7 microns in diameter. Separating this tow into smaller bundles always resulted in many stray filaments sticking out of the smaller bundle. It was necessary to smooth the small bundles manually. Resistance of the tow to separation made it very difficult to obtain bundles of the same size.

Another problem was poor wettability of the Morganite by the PL-1 matrix. Attempts to dissolve PL-1 in toluene and acetone to reduce the viscosity and to enhance migration of the solution into the Morganite bundle were not very successful. Partial or inconsistent cure of the PL-1 resulted in these cases. A process was developed for preimpregnating Morganite bundles before embedding them in plastic. This process involved:

1. Hanging Morganite bundles vertically
2. Putting PL-1 on the bundle and letting it flow over and among the filaments
3. Manually massaging the PL-1 into the bundle
4. Curing the bundles

Some success was obtained with this process. However, because of the tedious, time-consuming nature of this process, only a small number of Morganite-reinforced specimens were made. The aforementioned difficulties were not present with the fiberglass reinforcing elements.

UNIAXIAL TESTING

Several preliminary tests were performed to establish specimen configurations and tensile gripping devices. This ultimately led to uniform loading and fracture within the gage section in a large proportion of the tests conducted. Two specimen configurations were adopted: a 1/4-inch-wide bar for 0° fiber orientations and a 1/2-inch-wide bar for cross-ply fiber orientations. Both these configurations had 2-inch parallel-side gage sections and tab ends. Special wedge grips were employed in these tests. Utilization of these grips largely eliminated grip-related failures and facilitated application of uniform stresses within the gage section.

PHOTOGRAPHIC RECORDING

Photoelastic observations were made with a transmission polariscope. Circularly polarized light was used. Observations and photoelastic data recording were made with monochromatic light obtained by combining Wratten filters numbers 74 and 77A. The light source was a 1000-watt quartz-iodine tube.

A variety of photographic and optical techniques was employed in these investigations. The objective was to combine high magnification and resolution with high framing rate. The restricted field of view associated with high magnification often resulted in the relaxation of this objective.

The types of photographic coverage included:

1. Still—Sinar Optical Bench Camera 4 x 5
2. Motion
    a. Holcher 70 mm, 20 frames per second
    b. Milliken 16 mm, 400 frames per second

In some cases, a 400-per-second framing rate was not fast enough to stop the fracture action. A Fastax camera operating up to 7200 frames per second was available; however, at this rate, a maximum of only 2.8 seconds of film is available, and it was not possible to locate the fracture event in time that precisely.

LOAD INDUCED FLAWS

The first phase of these studies was concerned with reinforced (glass and Morganite) tensile specimens with no apparent initial flaws. Examination of these specimens on an optical comparator, set up as a transmission polariscope, revealed no significant initial stresses.

Fiberglass-Reinforced Composites

Six 0° fiberglass-reinforced specimens were subjected to axial tension. Fracture occurred very rapidly, and the action was not stopped by a Milliken camera operating at 400 frames per second. The average ultimate stress for five specimens (one specimen failing in the grips) was 18,700 psi. In each case a brittle-type failure occurred. A few small secondary cracks developed at the fibers near the main crack. Fracture was accompanied by unbonding of fiber bundles away from the fracture surface. Distinct residual stress patterns associated with the unbonded fibers were observed. A typical residual stress pattern is shown in Figure 2.

It was not possible to foresee the location or instant of impending fracture by photoelastic stress patterns, hence Fastax photographic recording was not attempted.

Five 0°-90° cross-ply fiberglass-reinforced specimens were subjected to axial tension to failure. Fracture generally took place more slowly than in the 0° specimens. Selected frames from a 70-mm film strip (taken with a Holcher camera operating at 20 frames per second) are shown in Figure 3. The series of pictures shows a sequence of failure propagation over a 0.5-second time interval. Two curved cracks (A), located on each side of the eventual failure surface, can be seen together with a small number of stacked, dish-shaped cracks. Note that the stacked cracks are in regions between transverse fiber bundles and are confined by these transverse fibers. A progressive unbonding emanating from the eventual failure surface and propagating away from this surface can be observed. Arrows in these pictures point to the fringe pattern caused by the unbonding.

Dish-shaped crack formations were present, to a greater or lesser extent, in all of the 0°-90° cross-ply specimens tested. Two cases of extensive stacked crack formations are presented in the posttest photographs of Figure 4. Several pertinent observations can be made from these photographs. Here, as in all other stacked crack formations, the dish-shaped cracks are concave toward the main fracture. Also, transverse fibers tend to inhibit the formation of these cracks.

It was observed in the 0°-90° cross-ply specimens that the main crack propagation path always passed through a transverse fiber bundle. The average ultimate stress for the five specimens tested was 8350 psi; however, considerable scatter is evident (maximum 9460, minimum 7380).

Tensile specimens having glass fiber orientation of $\pm 45^{\circ}$ demonstrated some basically different failure characteristics. Failure always initiated at locations where fiber bundle crossover points were at or near the edge of the specimen (arrow in Figure 5). The basic mechanism of failure was shear along the fibers. This was accompanied by local stacked cracks at the crossover point and some unbonding along the fiber bundles intersecting at the crossover point.

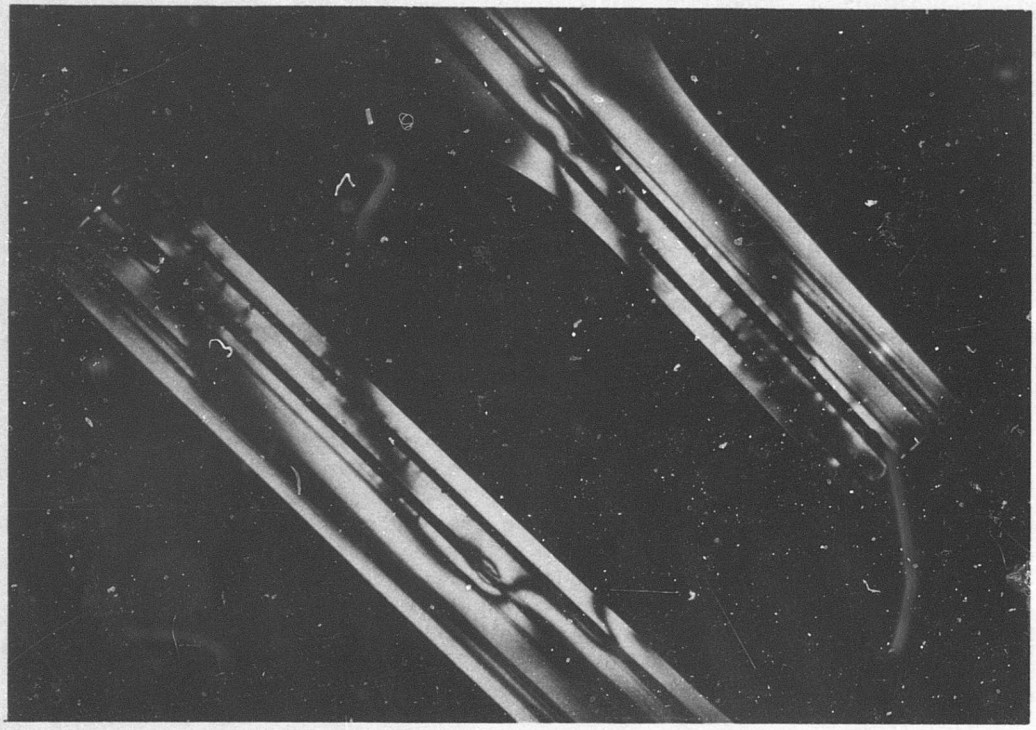

Figure 2. Residual Stresses in Unidirectional Fiberglass-Reinforced Tensile Specimen Showing Unbonding of Fiber Bundles (1.8X).

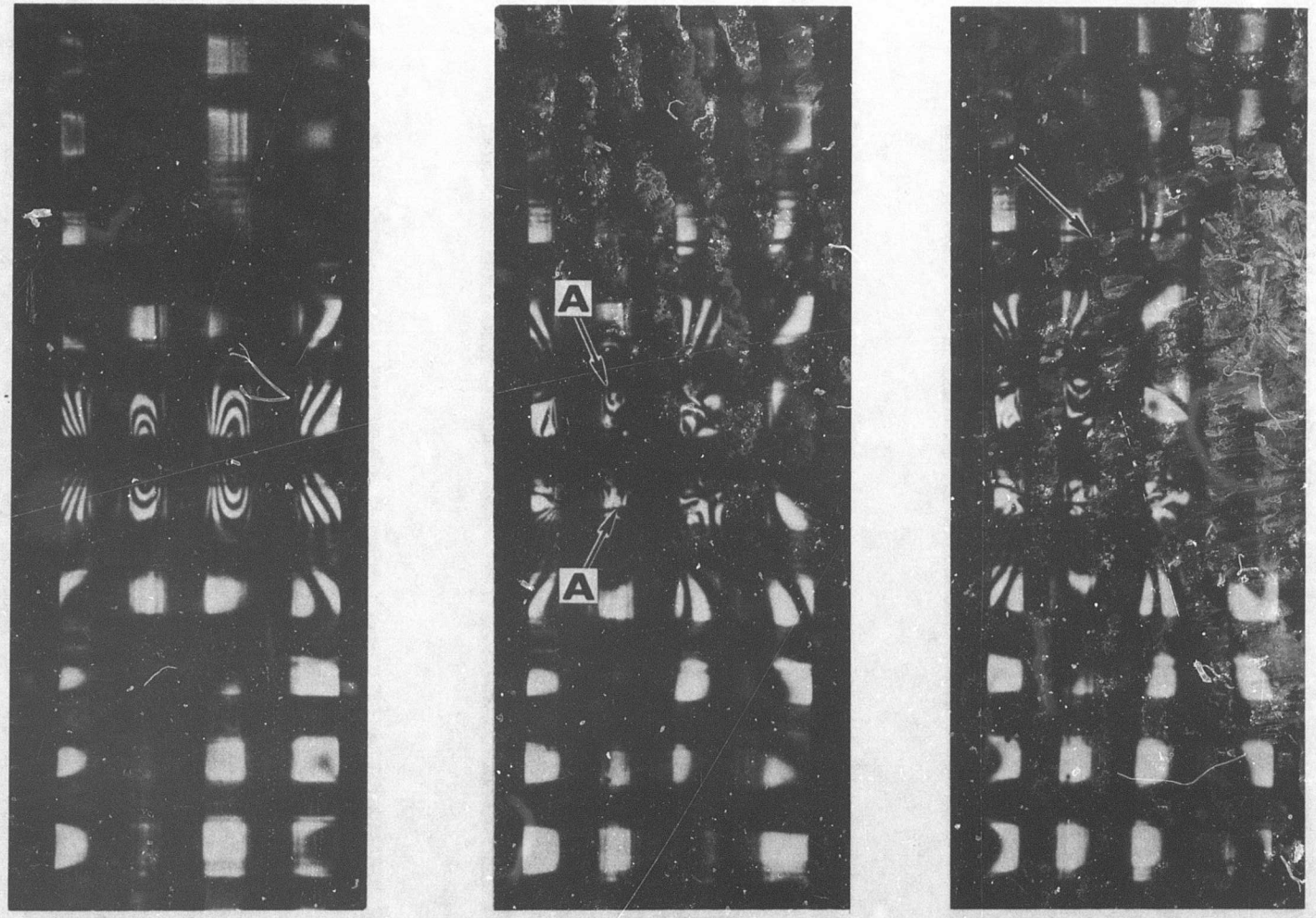

(a) (b) (c)

Figure 3. Tensile Failure Sequence of 0°-90° Fiberglass-Reinforced Specimen (3.8X).

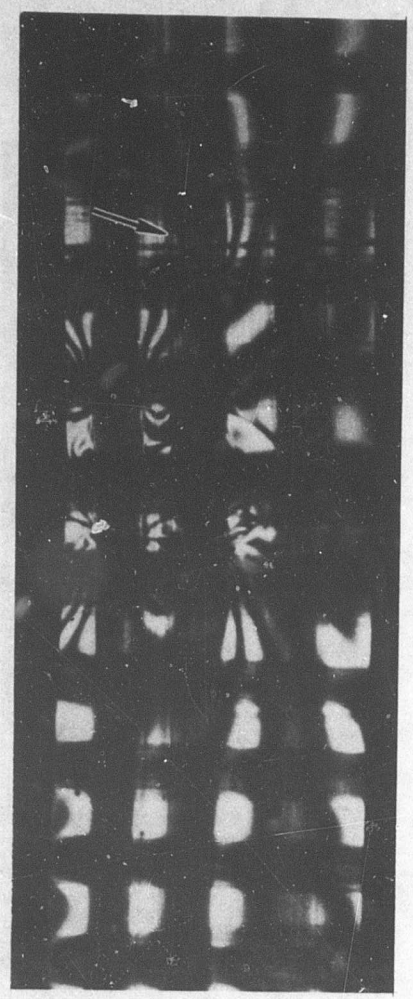

(d)

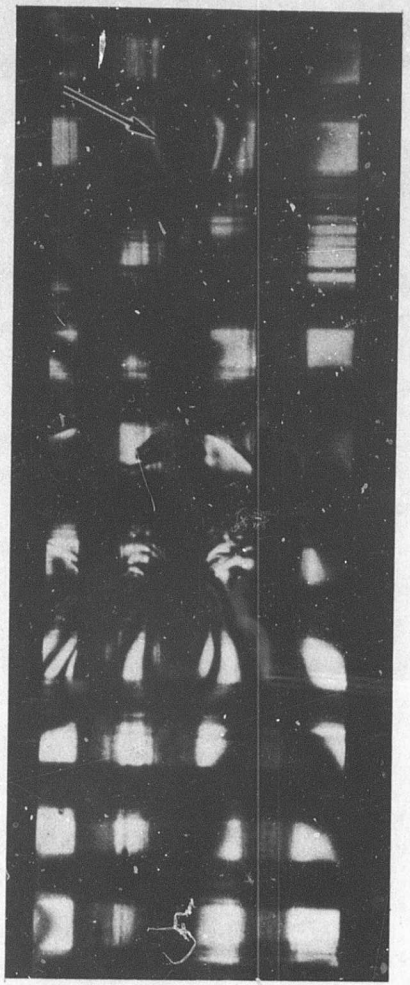

(e)

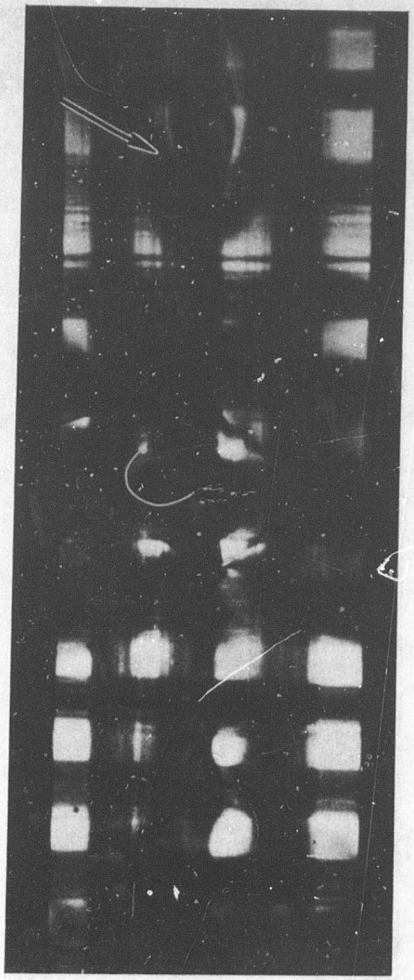

(f)

Figure 3. (Concluded).

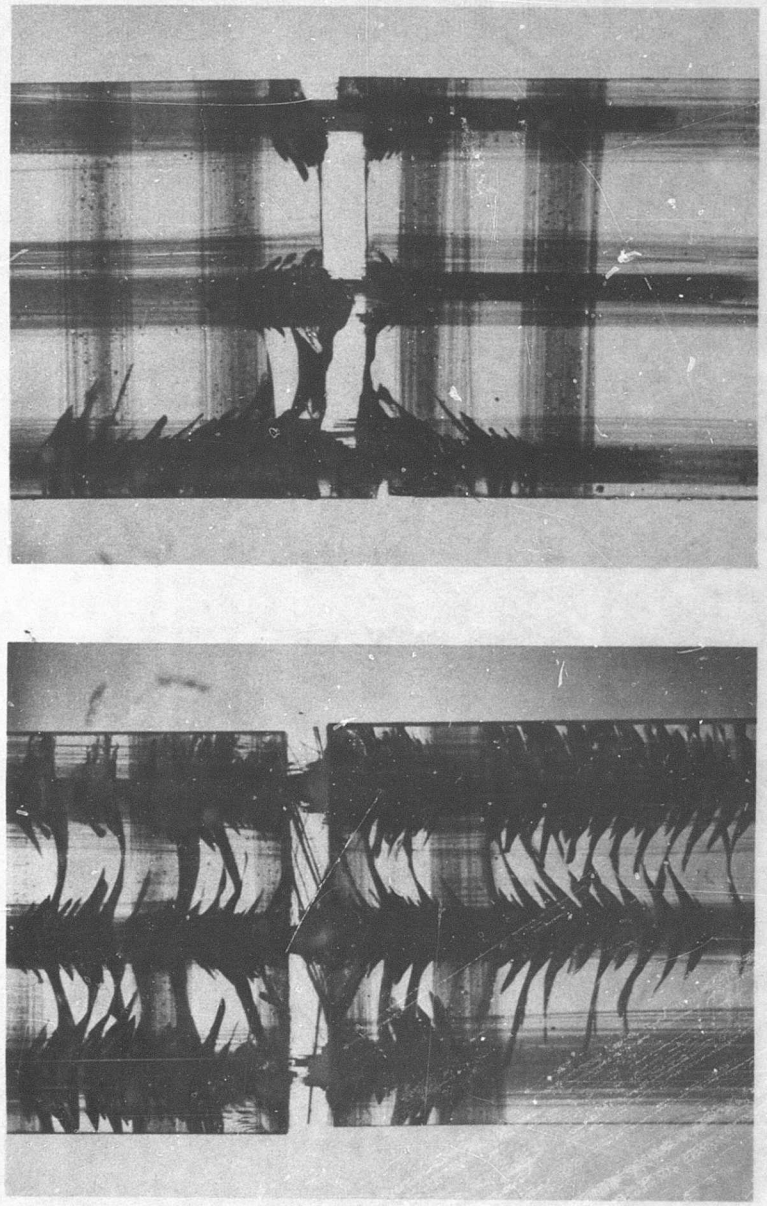

Figure 4. Posttest Details of Stacked Crack Formations in a 0°-90° Fiberglass-Reinforced Specimen (5.1X).

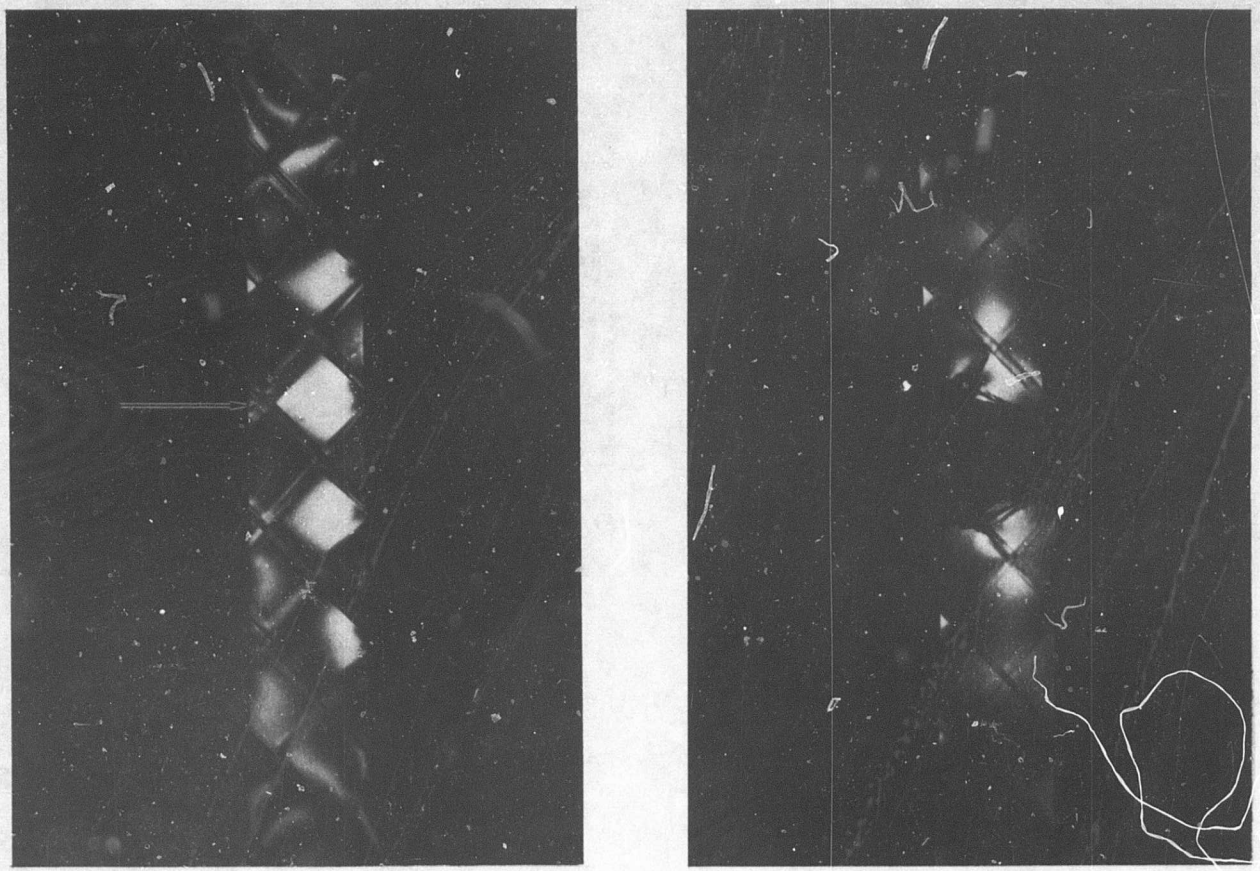

Figure 5. Failure of $\pm 45^{\circ}$ Cross-Ply, Fiberglass-Reinforced Tensile Specimen Initiated at Fiber Bundle Crossover (1.4X).

Morganite-Reinforced Composites

As was mentioned previously, considerably difficulty was encountered with wetting of Morganite by PL-1 plastic. Although individual preimpregnating of Morganite fiber bundles with PL-1 alleviated this difficulty, subsequent testing revealed indications of an interface between the preimpregnated bundles and the bulk matrix material.

In Figure 6, a Morganite-reinforced specimen is under tension. For this specimen, several individual Morganite fibers were carefully separated from the large tow of fibers. Portions of the fibers became unbonded from the matrix. In these regions, many very fine cracks developed normal to the fibers. A detail of the cracked and uncracked regions is presented in Figure 7. Ultimate failure took place within the grips.

Morganite-reinforced specimens with larger fiber bundle size were also tested. Failures of these specimens were of a brittle fracture type. There was little tendency to form arrays of secondary cracks. Some isolated secondary cracks developed close to the main crack surface. Some were parallel to the fiber and some normal to the fiber. An example is shown in Figure 8 (the crack parallel to the fiber is obscured by the fiber). Fiber pullout is also evident. Posttest examination revealed only a low-order, rather uniform residual stress field. It is to be noted that this specimen was not made with preimpregnated fiber bundles, and examination of the failure revealed that the interior of the bundle had little or no matrix.

A 0° Morganite-reinforced specimen containing preimpregnated fibers is shown in Figure 9. The complex stress pattern shown in this photograph was caused by successive unbonding of various regions of the three fiber bundles. The stress pattern was visually observed to develop in one region, skip to another, etc., until the pattern shown appeared. Failure occurred when unbonding extended over the entire specimen.

Failure of the 0°-90° Morganite-reinforced specimens was similar to that of the glass-reinforced specimens, in that fracture always occurred through a transverse fiber bundle. The stress pattern before failure was very similar to that shown in Figure 3a. No stacked, dish-shaped cracks were observed with Morganite-reinforced specimens. There was no evidence of unbonding of fiber bundles prior to fracture.

INITIAL FLAWS

Several types of initial flaws were incorporated into reinforced composite specimens during fabrication. The flaws investigated were (1) voids, (2) contaminated fiber surfaces, and (3) damaged fibers. The anticipated profound effect of flaws on failure and strength characteristics was confirmed in some cases.

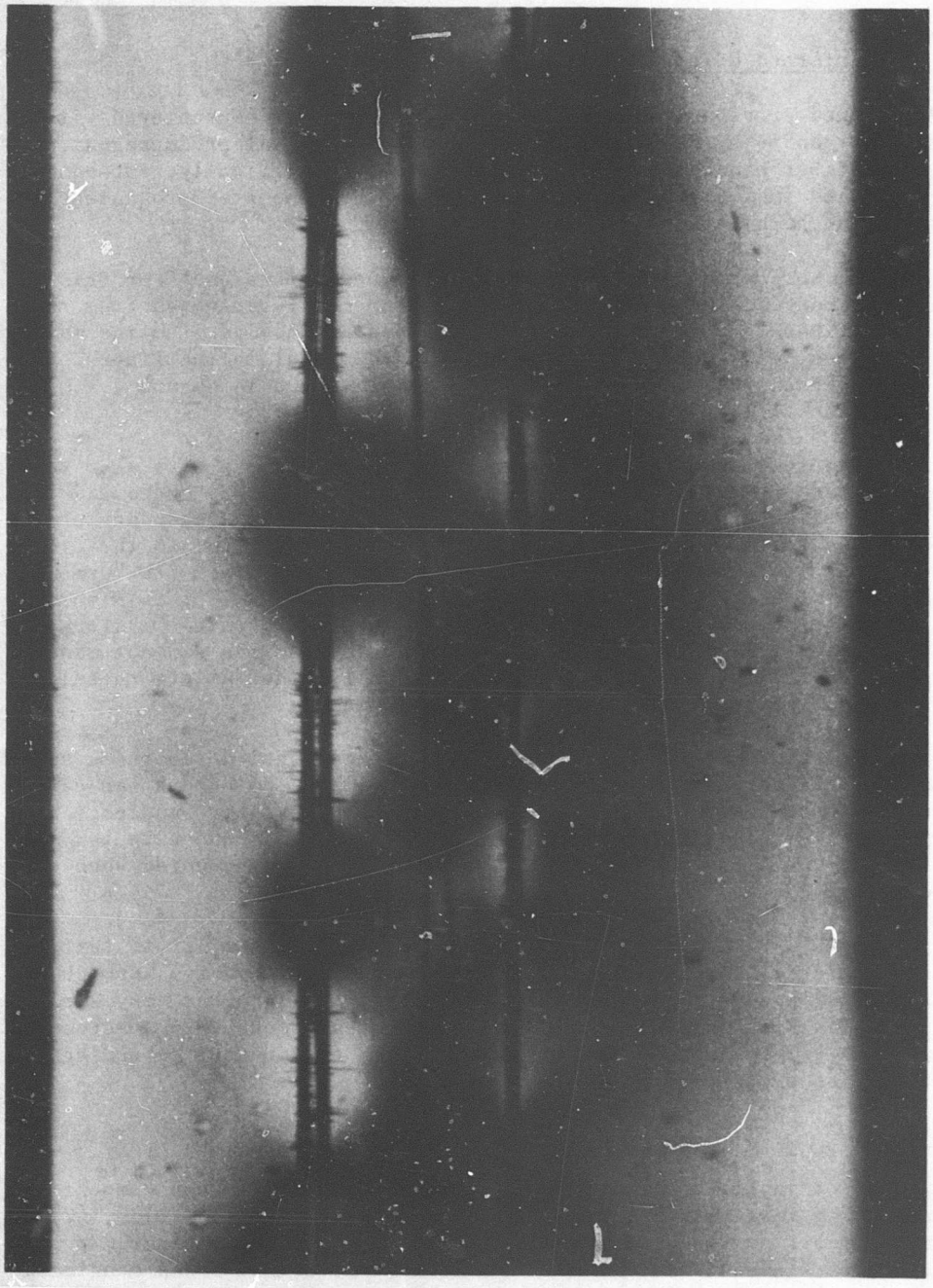

Figure 6. Matrix Cracks in 0^{o} Morganite Tensile Specimen (20X).

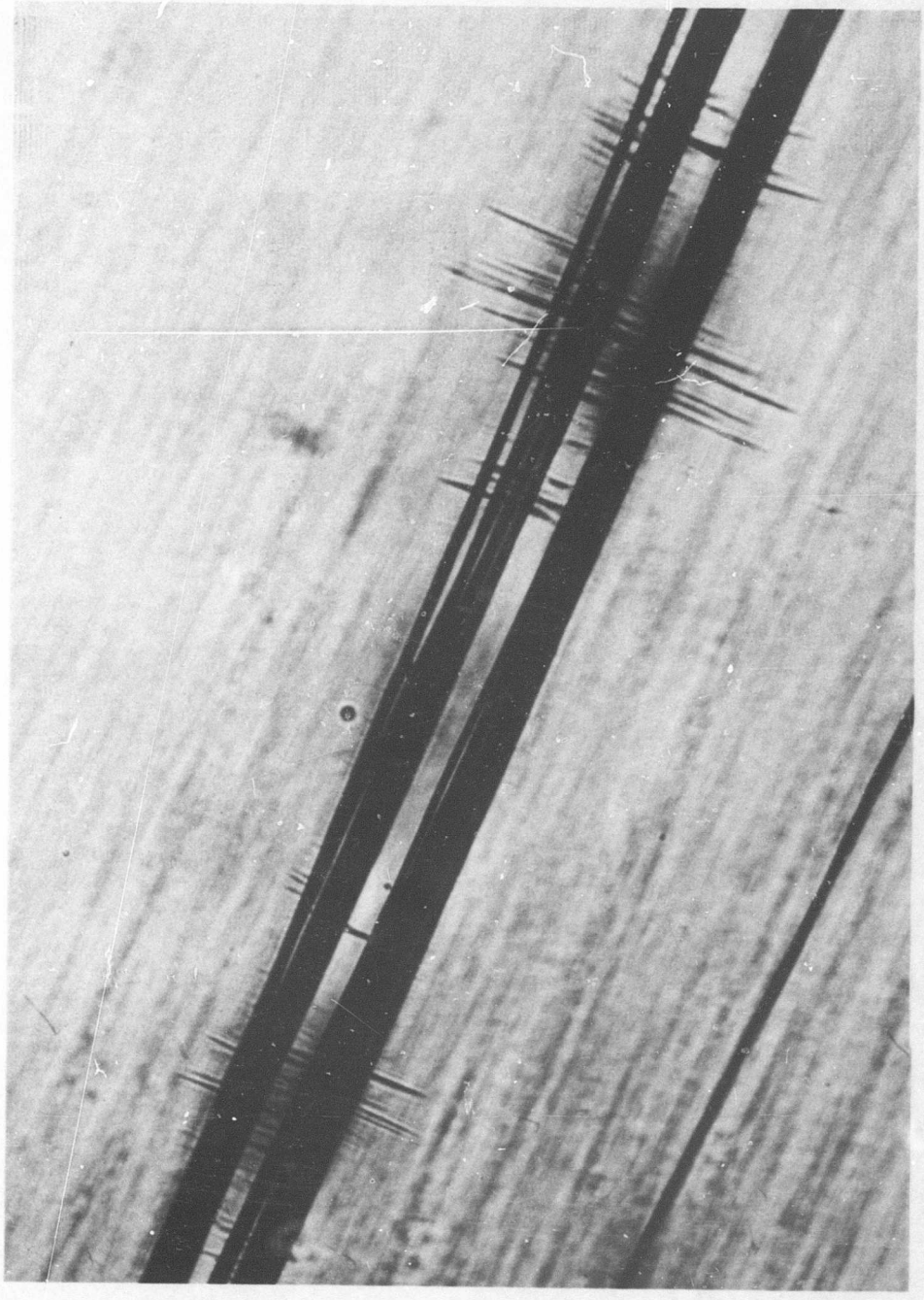

Figure 7. Detail of Matrix Cracks Shown in Figure 6 (100X).

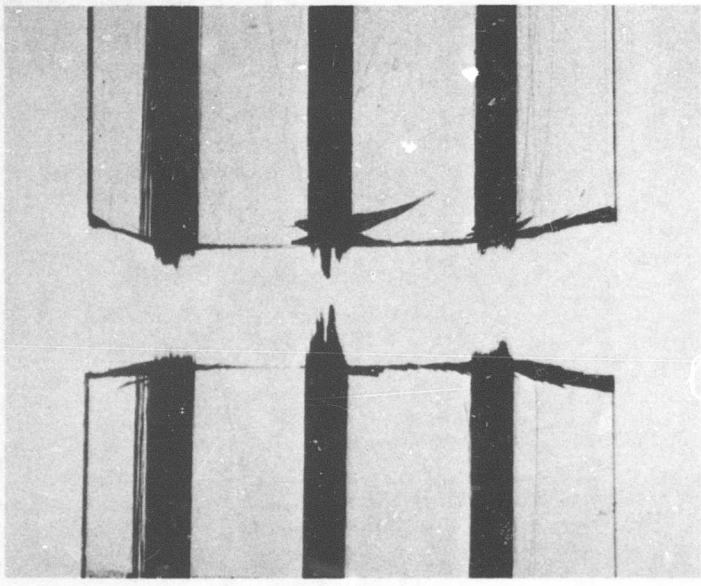

Figure 8. Posttest Detail of Morganite-Reinforced Tensile Specimen (6.4X).

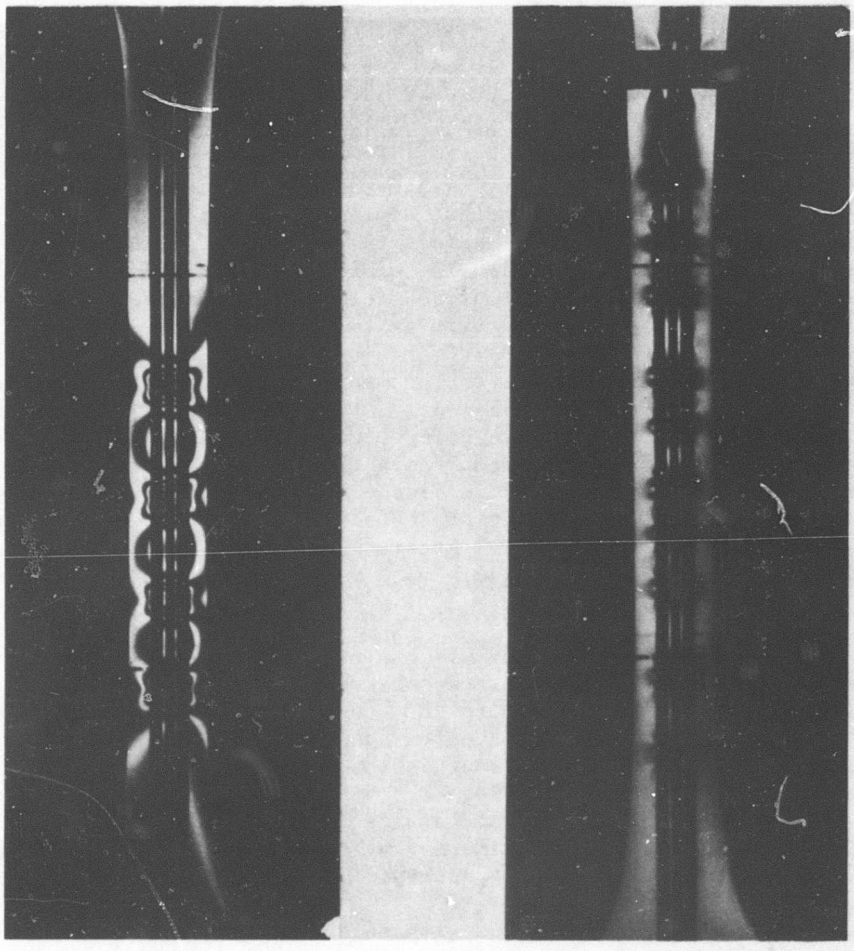

(a) (b)

Figure 9. Unbonding Around Morganite Fiber Bundles (1X).

Fiberglass-Reinforced Composites

The effect of voids on the behavior of 0° fiberglass-reinforced specimens varied considerably with the size of the void. Usual fabrication processes often resulted in microvoids between ends of the 12-end fiberglass roving. The stress concentrations associated with these microvoids, under a tensile field, were observable when appropriate optics were employed. However, microvoids appeared to have little effect on the path of catastrophic crack propagation. Somewhat larger voids also exhibited classical photoelastic stress patterns in a macroscopic tension field. The effect of these voids depended to some extent on their proximity to fiber bundles.

An example of the effects of a cluster of macroscopic bubbles in the vicinity of fiber bundles is presented in Figure 10. A remarkable alteration of the behavioral pattern of 0° fiberglass-reinforced specimens can be observed here. Whereas all previously tested 0° specimens exhibited no stacked crack formations, the specimen presented in Figure 10 developed a very intricate array of stacked cracks. Unbonding of the central fiber bundle occurred after formation of the stacked crack array. An average ultimate stress for three specimens with large voids was 13,360 psi, compared with 18,700 psi for five unfaulted specimens.

The effect of a damaged filament bundle can also be expected to depend on the extent of the damage. To ensure an observable effect in this work, approximately one third of the fibers in a central bundle were cut. As the specimen was loaded, stress concentrations were evident at the cut filament site. Two specimens, of the four tested, failed with a crack propagating through the cut filament site. The other two specimens experienced uneven loading, and failure occurred outside the gage section. The average stress at failure for the two specimens was 14,400 psi. No stacked crack formations were observed in these specimens.

Specimens having fibers contaminated with mold release showed no dramatic alteration of failure pattern or ultimate tensile strength compared with the uncontaminated 0° specimens.

Initial flaws did not appear to alter the behavior of the 0°-90° glass-reinforced specimens. An example of this is presented in Figures 11 and 12. This specimen contained clusters of bubbles, some of which were quite large. Failure initiated at the edge of the specimen at a transverse fiber bundle. Little difference could be seen between the ultimate stresses in 0°-90° specimens with flaws (voids, cut and contaminated fibers) and those without flaws. In every case, failure initiated at transverse fiber bundles.

Two specimens reinforced with glass fibers at $\pm 45^{\circ}$ and containing bubbles were tested. Both these $\pm 45^{\circ}$ specimens exhibited extreme sensitivity to the presence of voids. Figures 13 and 14 illustrate this significant aspect of composite behavior. Failure was a shear type and was accompanied by local stacked cracks at crossover points and some unbonding away from the crossover points.

(a) (b) (c)

Figure 10. Influence of Large Bubbles on Failure of Fiberglass-Reinforced Tensile Specimen (1.1X).

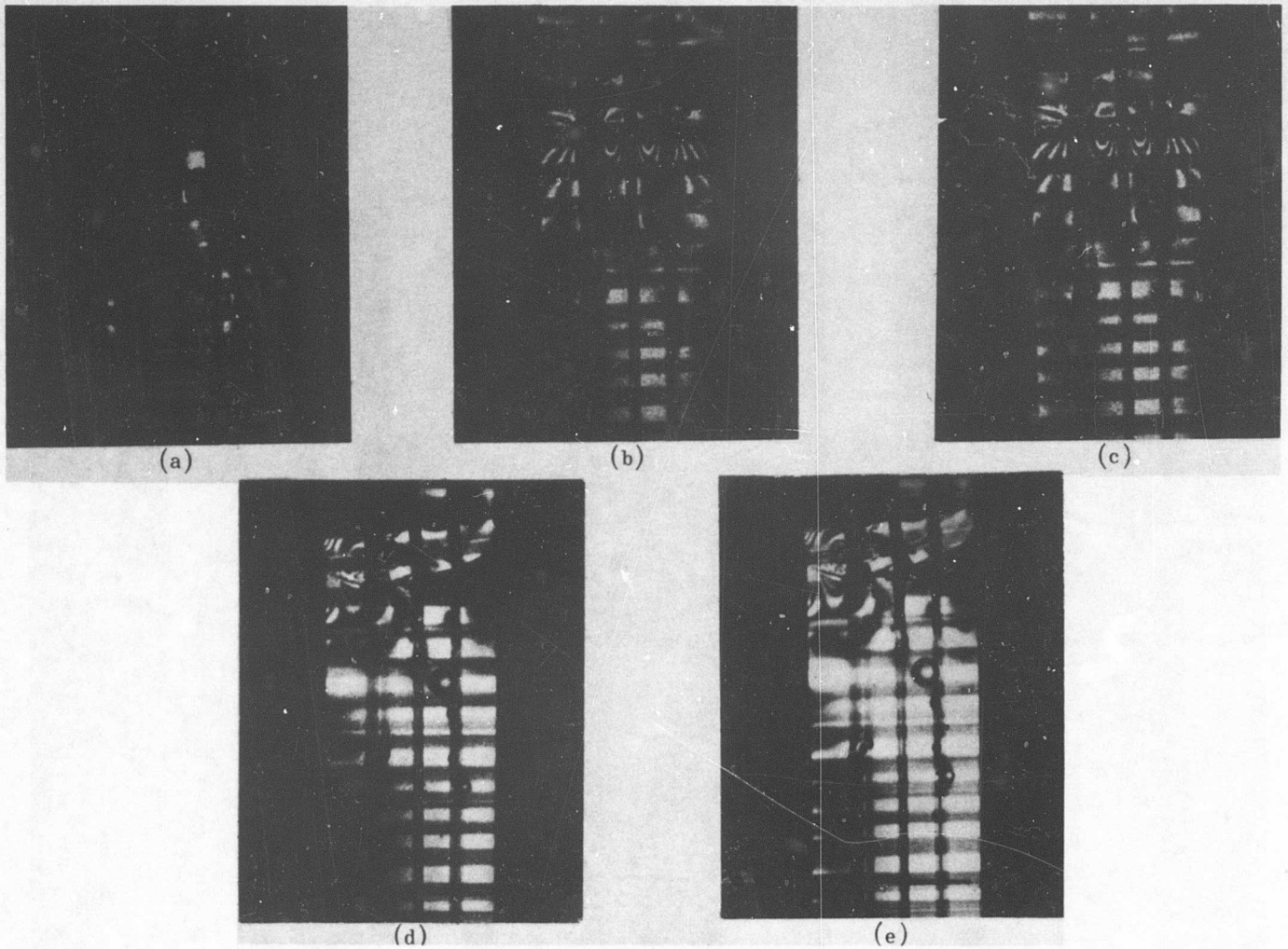

Figure 11. Cross-Ply Fiberglass Uniaxial Tensile Test (2.2X).

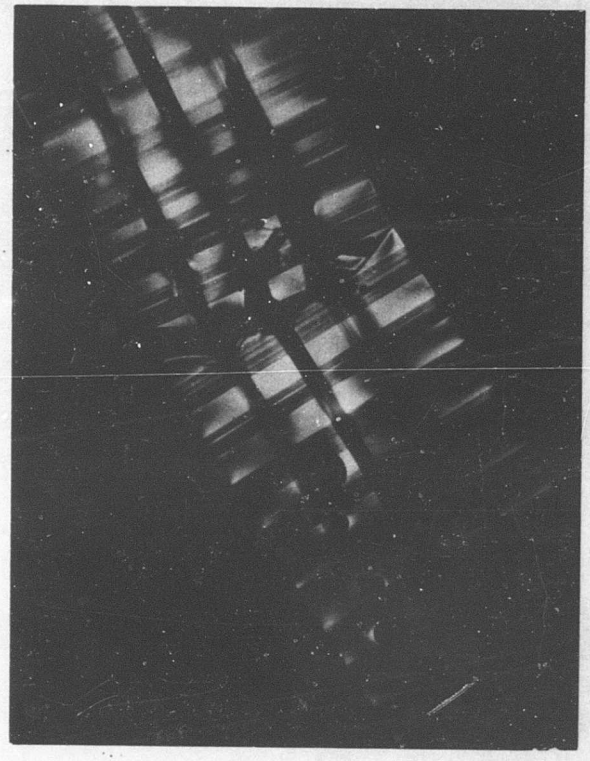

Figure 12. Posttest Closeup of Fiberglass Specimen Shown in Figure 11 (3.4X).

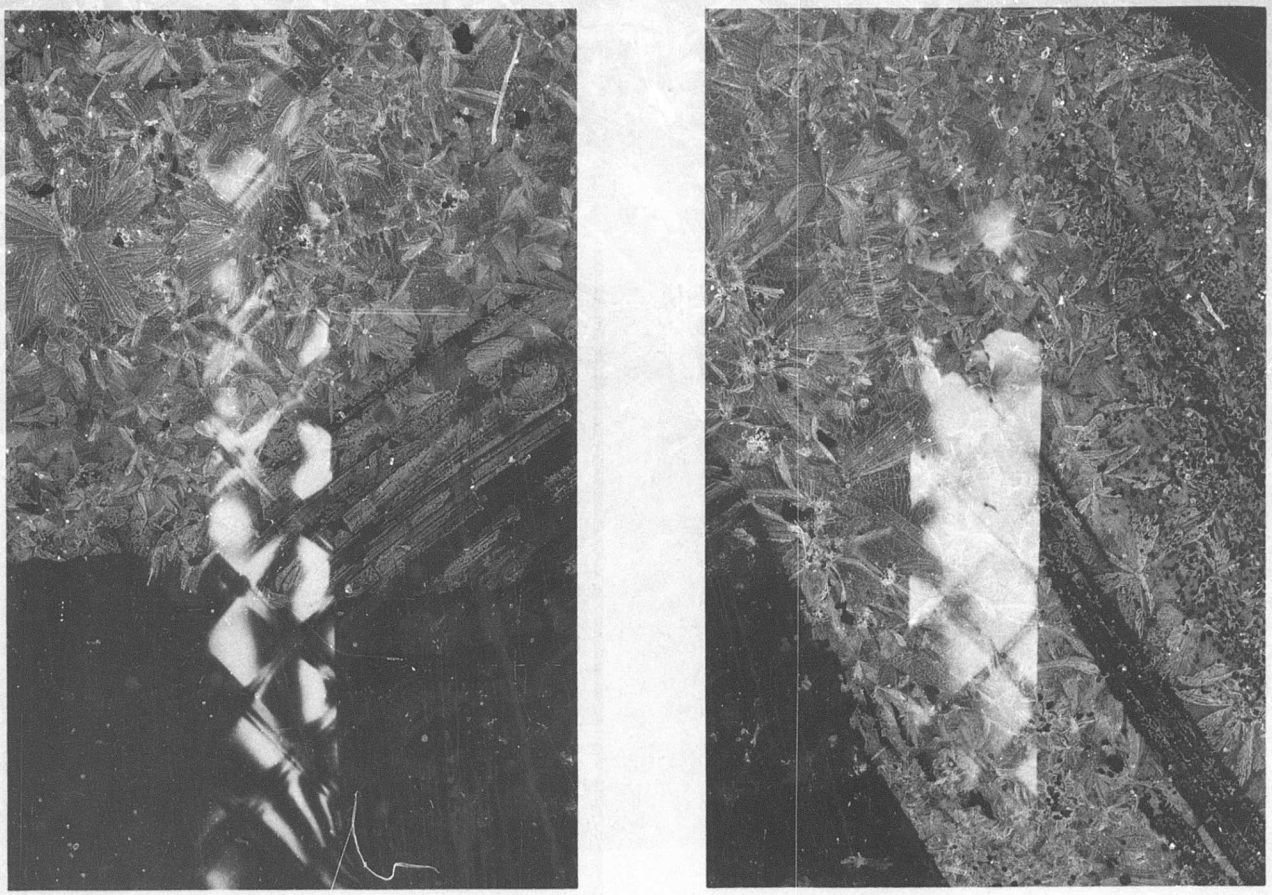

(a) (b)

Figure 13. Failure Initiated by Bubbles in $\pm 45^{\circ}$ Cross-Ply, Fiberglass-Reinforced Tensile Specimen (1.6X).

(b)

(a)

Figure 14. Failure Initiated by Bubbles in $\pm 45^{\circ}$ Cross-Ply, Fiberglass-Reinforced Tensile Specimen (1.6X).

Morganite-Reinforced Composites

The difficulties encountered in fabrication of Morganite-reinforced composites make assessment of the effects of flaws somewhat inconclusive. However, some observations can be made. In all cases where there were damaged fiber bundles (damage caused by cutting approximately 1/3 fiber bundle), fracture occurred through the damaged fiber site. The concentrated stress pattern seen in Figure 15a is due to the damaged fiber bundle. Figure 15b shows a brittle-type fracture passing through the region of damage. Although there was considerable scatter in the ultimate stress values for the Morganite-reinforced specimens, damaged fiber bundles distinctly reduced the load carrying capacity.

A very interesting crack growth formation was observed in the vicinity of a void in a 0° Morganite-reinforced specimen. Figure 16a shows a stress pattern around the void similar to the classical pattern found around a hole in a plate subjected to tension. The arrow in Figure 16b points to the tip of an advancing crack. Figure 16c shows the fully developed crack curving away from the void. Final specimen failure occurred at the grips. A posttest high-magnification photograph of the void region is presented in Figure 17. Examination under the microscope revealed that there was no fiber fracture in the vicinity of the void or cracks.

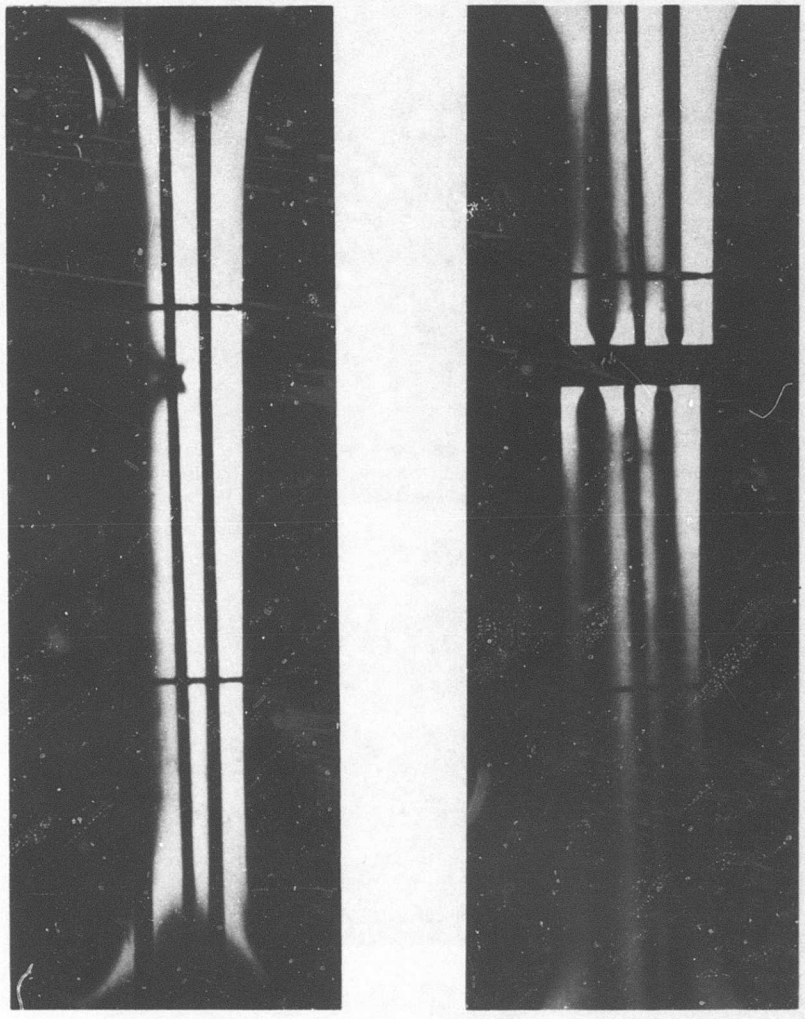

(a) (b)

Figure 15. Influence of Damaged Morganite Fiber Bundle On Failure (1.7X).

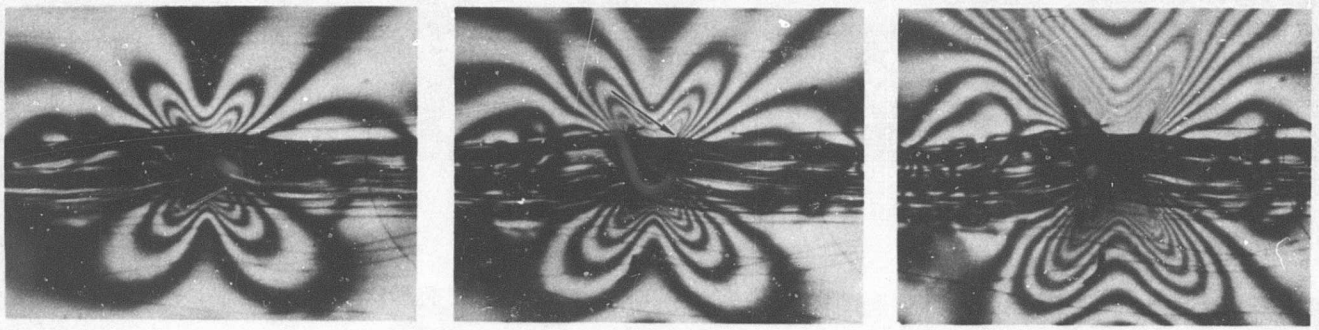

(a) (b) (c)

Figure 16. Crack Formations Near Void in Morganite-Reinforced Tensile Specimen (6.6X).

Figure 17. Posttest Detail of Void and Cracks in Morganite-Reinforced Tensile Bar (35X).

BIAXIAL TESTING

Studies into the behavior of reinforced composites under biaxial stress fields involved two types of specimen configurations: disks and flat plates. The disks were subjected to diametral compression, which results in a compression-tension field at the disk center. The short, wide, flat plates were subjected to tension applied to the wide plate edge. A tension-tension field results at the center of the plate. This test is commonly called the biaxial strip test.

Table II describes the types of biaxial specimens tested. Only load-induced flaws were considered in this phase of the investigation.

TABLE II. BIAXIAL TEST SPECIMENS

	Disks	Plates
Glass		
0°	X	X
0°-90°	X	X
±45°	-	X
Morganite		
0°	X	-
0°-90°	X	-
±45°	-	-

DISKS

Initial tests were performed on free-standing disks. Buckling of the disk invariably occurred before internal failure of the disk was achieved. This problem was partially solved by reducing the disk diameter from 1.12 inches to 3/4 inch. The remaining difficulty was overcome by providing lateral support to the disk. The lateral support members were optically clear and stress-free so as not to confuse photoelastic observations.

Three unidirectional fiberglass-reinforced disks were tested to failure. As the diametral compressive load was applied to each of these disks, a crazing became apparent toward the center. This crazing was accompanied by a lower rate of load increase (under constant crosshead rate). Further loading resulted in vertical cracks (i.e., perpendicular to the induced tensile stress) through or near fiber bundles. Figure 18 shows a 0° fiberglass-reinforced disk just after failure while still under load. The lack of clarity in the central region of the disk is caused by matrix crazing.

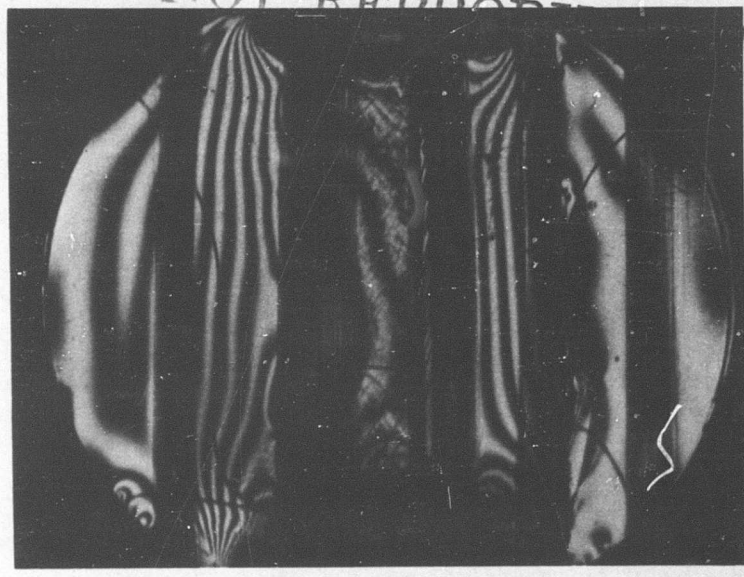

Figure 18. Unidirectional Fiberglass-Reinforced Disk Failing Under Diametral Compression (5.5X).

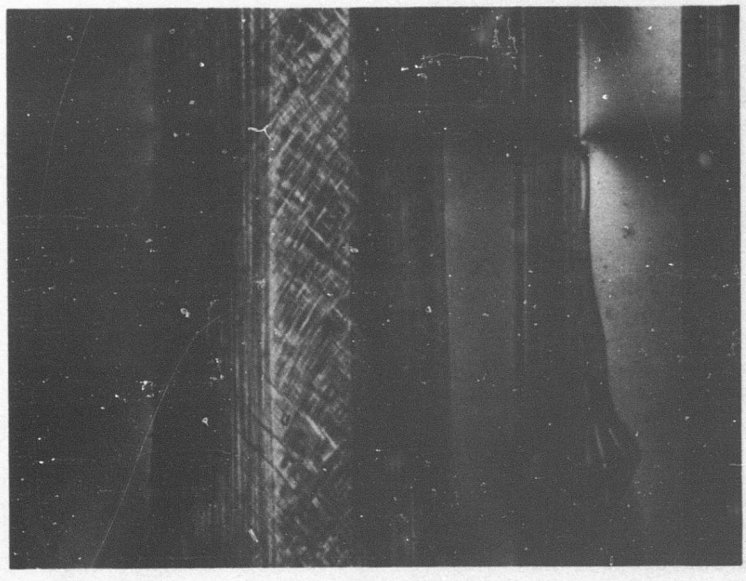

Figure 19. Posttest Detail of Failed Disk (8X).

Figure 19 is a posttest detail of the crazed region. It can be observed in both these photographs that the crazing tends to be confined by the adjacent fiber bundles.

Several aspects of failure in the Morganite-reinforced disks were observed to be different from those in the fiberglass disks. Figure 20 shows the diametral compression of a 0° Morganite-reinforced disk. Some unbonding developed at very low load at the central fiber bundle near the center of the disk. Figures 20a and 20b show fiber bundles away from the central one progressively exhibiting unbonding with increasing compressive load. The crazing phenomenon described above is also apparent in these photographs. It can be seen that the matrix crazing of the Morganite-reinforced disk is much finer than that observed in the fiberglass-reinforced disk. Again, the crazing is confined between the two fiber bundles adjacent to the central one. A large vertical crack finally propagated within the central fiber bundle. Large secondary fractures can be seen at the left in Figures 20c and 20d. Figure 20d is a posttest study made with transmitted, polarized light.

Two 0°-90° Morganite disks were also tested. An internal failure was generated in one of these specimens. This failure, a vertical crack along the diameter accompanied by unbonding, was different from the failures described above. The crack was not within a vertical fiber bundle. Its path of propagation crossed five horizontal fiber bundles causing fracture and some pullout of these bundles. The unbonding in this specimen occurred at the horizontal fiber bundles in the vicinity of the vertical crack.

Testing of the second 0°-90° disk was terminated before failure because of interference between the lateral support fixture and the loading head. However, careful examination of this specimen revealed the initiation of some unbonding along the horizontal fiber bundles near the vertical diameter of the disk. The start of very small matrix cracks at the unbonded region was also observed.

BIAXIAL TENSION STRIPS

The first biaxial strip test specimen was fiberglass-reinforced with a 0°-90° fiber orientation. Stainless-steel doublers were bonded to the specimen with epoxy 820 and then bolted. Specimen dimensions between doublers were 5.82 inches by 1.25 inches by 0.085 inch. The specimen and doubler assembly is shown in Figure 21. Testing was performed on an Instron machine. Uniform loading was obtained until a bond failure between the doubler and specimen occurred. Posttest examination revealed that after bond failure the load was unequally distributed among the bolts, resulting in the failure shown in Figure 22.

Even though failure was not achieved in the central gage region, some observations can be made about a propagating crack in the 0°-90° fiber configuration. The crack propagation trajectory was substantially parallel to the horizontal fiber bundles. Stacked cracks were evident at vertical fiber bundles near the main crack. Also, there was unbonding of several vertical fiber bundles away from the propagating crack.

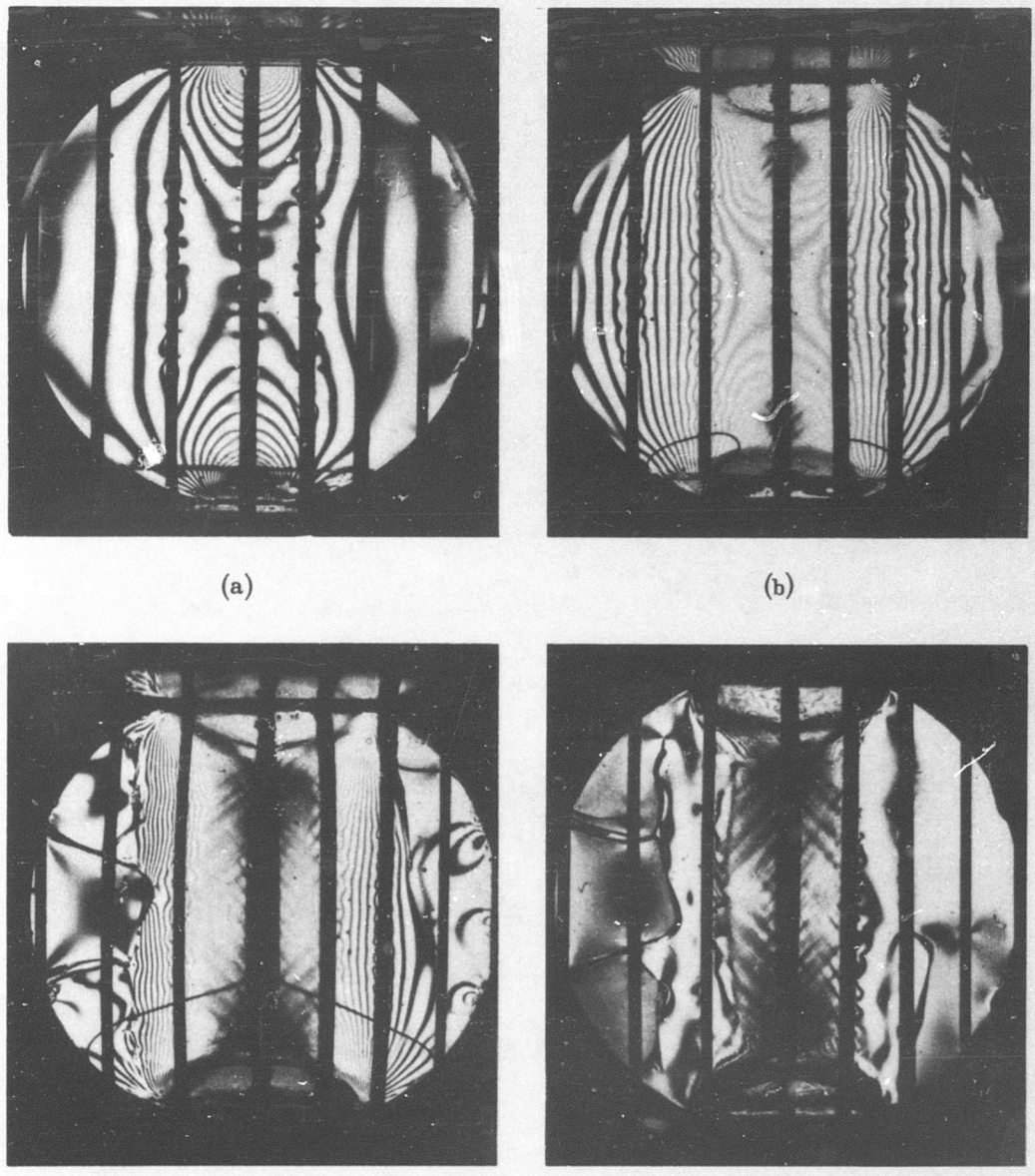

(a) (b)

(c) (d)

Figure 20. Failure of Unidirectional Morganite-Reinforced Disk Under Diametral Compression (3.7X).

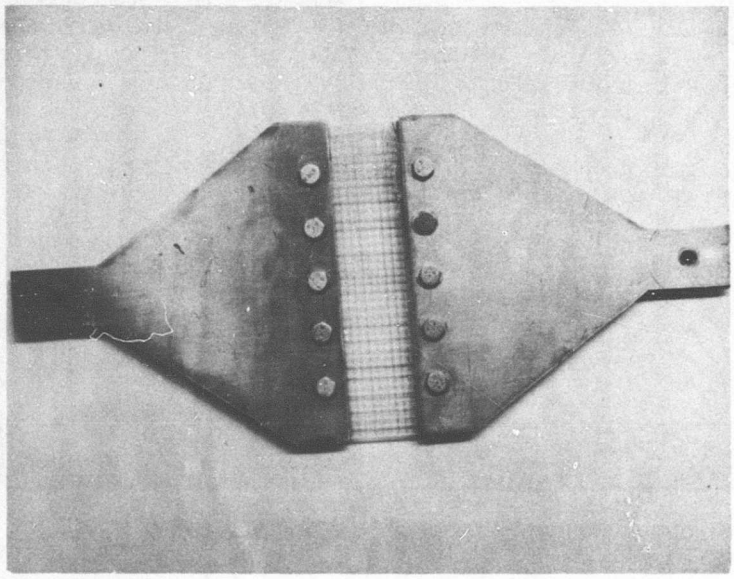

Figure 21. Biaxial Strip Test Setup (0.33X).

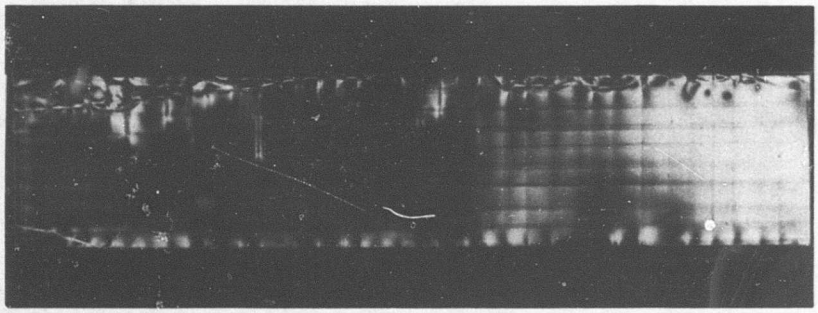

Figure 22. Posttest Condition of Biaxial Strip Specimen—Circularly Polarized Light (0.83X).

An attempt was made to reduce the stiffness mismatch between the doubler and the specimen by tapering the doubler. The tapered doublers were then attached to a 0° fiberglass-reinforced specimen by means of epoxy 820 and bolts. A larger bond area between the specimen and doublers was provided.

In Figure 23a, the specimen is seen to have a uniform stress pattern in the central region of the plate. However, premature failure initiated in the upper left corner of the plate and propagated toward the right. Loading was continued, and an interesting sequence of photographs (Figures 23b through 23d) was obtained. Stacked crack formations can be observed where the many cracks cross the vertical fiber bundles. Previous evidence (uniaxial tests) that stacked crack formation occurred after passage of the main crack was visually confirmed. No fiber unbonding was apparent.

A very important aspect of this crack propagation test is the crack bifurcations which occur at fiber bundles. Most current analytical crack propagation studies of anisotropic materials consider the propagation of a single crack which does not change direction. The observations made in this test indicate that this analytic approach may be in serious error. Recognition of the importance of crack bifurcation has recently been reported by Smith (Ref. 4).

Further modification of end-fixture attachments was attempted to achieve failure in the gage region. An approach was adopted which utilized tapered plastic plates bonded between the steel doublers and the reinforced plate specimen. The entire end assembly was then bolted. Glass fiber-reinforced plates of $\pm 45^{\circ}$ and 0°-90° orientation were tested using this approach. Figure 24a shows the $\pm 45^{\circ}$ specimen under low load. Channeling of the stresses by the $\pm 45^{\circ}$ fiber orientation is clearly evident in this photograph. Further loading caused a grip failure, which initiated at a bubble within the region where the tapered plastic piece was bonded to the specimen. Loading was continued and complete failure was achieved. Noteworthy in the failure is the fact that the crack trajectories almost invariably passed through fiber bundle crossover points. Stacked cracks were evident at these crossover points. Also important are crack bifurcation and, in some cases, two cracks coalescing to form one crack. Some unbonding away from the advancing crack can be seen.

The 0°-90° plate tested with this last end-fixture modification failed completely in the grips.

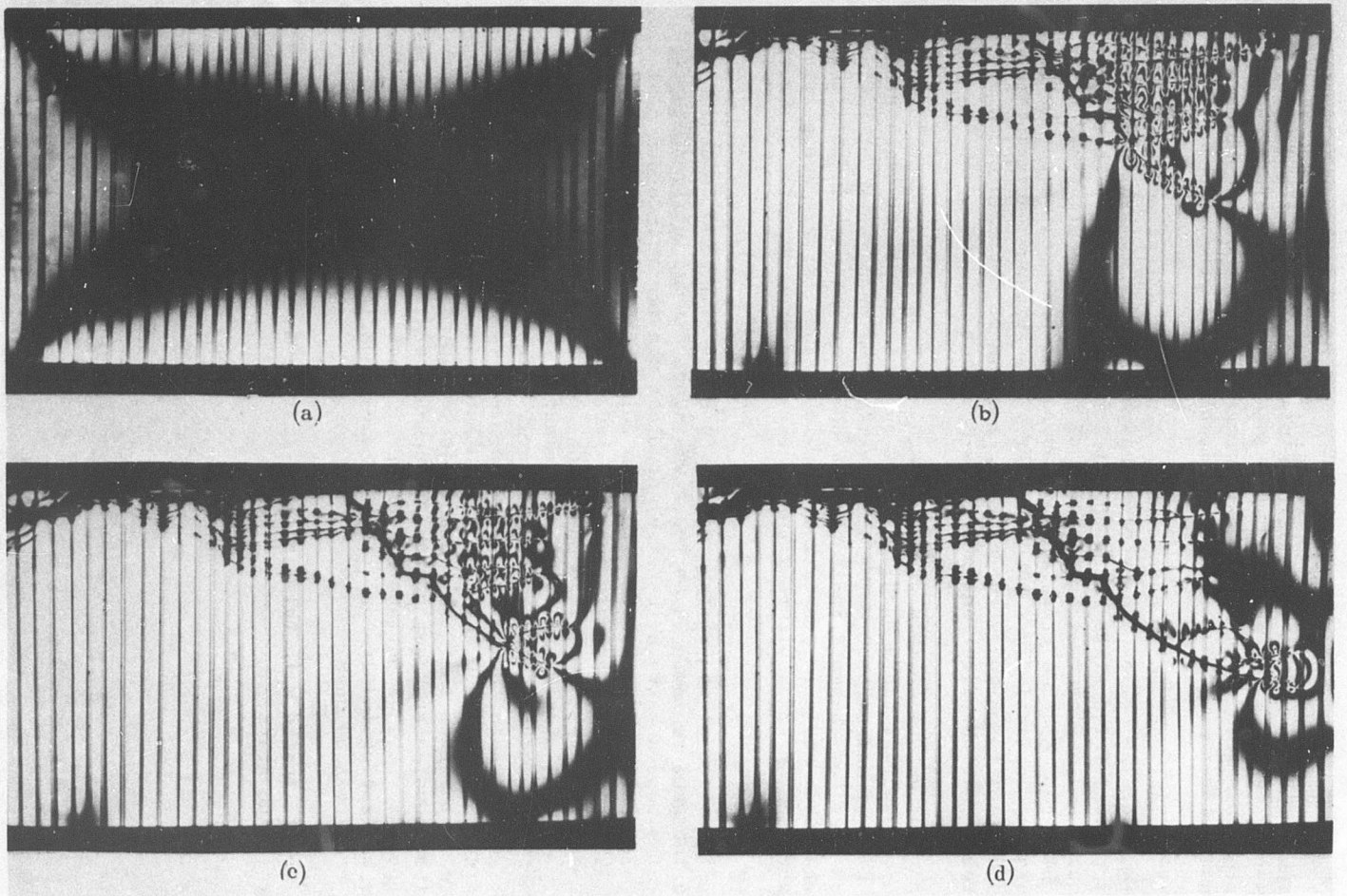

Figure 23. Failure of Unidirectional Fiberglass-Reinforced Biaxial Tensile Strip (0.76X).

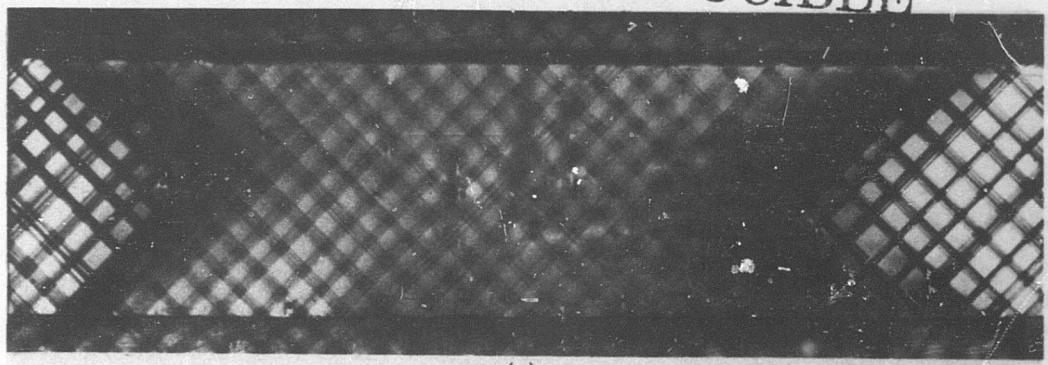

(a)

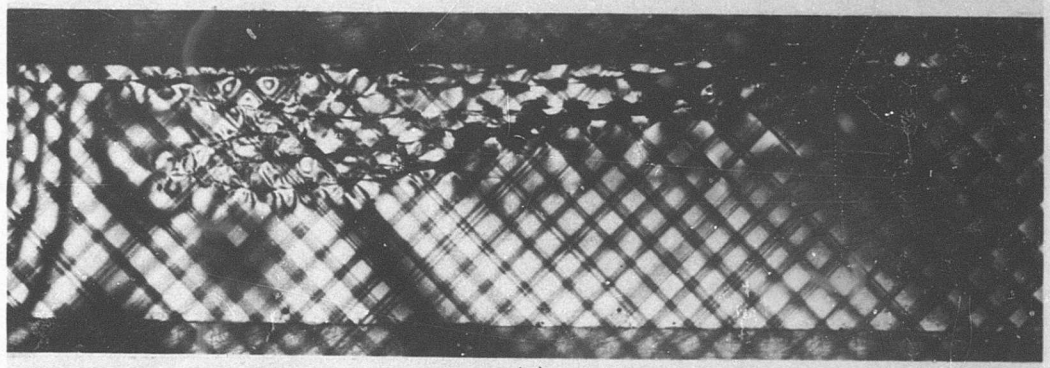

(b)

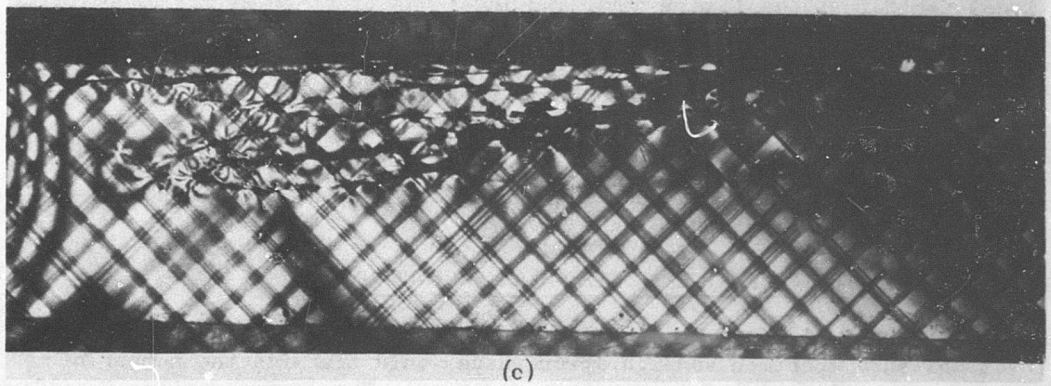

(c)

Figure 24. Failure of $\pm 45^{\circ}$ Glass-Reinforced Biaxial Strip Specimen (1.6X).

CYCLIC TESTING

Because many structural applications of reinforced composites involve repetitive loadings, a special cyclic loading apparatus was designed and fabricated to study this important phase of structural behavior.

CYCLIC TESTING APPARATUS

The apparatus used to provide cyclic loading is a Rocketdyne-designed low-frequency cyclic fatigue machine. This device utilizes the "scotch yoke" principle to convert a controlled rotary motion into a pure sinusoidal rectilinear motion. This motion is transmitted through an adjustable driver to a test specimen suspended between a rigid mounting fixture and the driver (Figure 25).

Torque was supplied by a 3/4-hp master shunt-wound, 115-volt ac, 60-cycle motor having a nominal speed range of 60 to 2500 rpm. Speed control was provided by a matched controller converting ac to dc for full-wave armature supply and excellent motor regulation.

A unique feature of this apparatus is the measurement of applied specimen loads using a force transducer mounted in series with the test specimen. A small universal bidirectional transducing cell with a 100-pound-capacity load cell accessory mounted at the fixed end of the specimen obtained this measurement. In addition, special cyclic test specimen holders and serrated specimen grips were designed to achieve a uniform uniaxial loading within the test section.

The desired variation in applied loads was obtained by adjusting the mechanical displacement of the rotating driver relative to the scotch yoke. Additional control of the loading mode and level was provided by the mounting fixture, which can be relocated, in line, over a wide range. Consequently, any desired level of preload could be obtained in tension-tension, tension-compression, or compression-compression modes.

Actual performance of this device exceeded design requirements. A frequency range of 0.5 to 42 cps was recorded, and loads in excess of 110 pounds were satisfactorily imposed on composite specimens. The maximum sinusoidal displacement obtainable was 0.5 inch.

CYCLIC TESTING OF COMPOSITES: FIBERGLASS REINFORCED

A preliminary test series was performed to establish test procedures and to establish a specimen configuration which would minimize the number of failures directly related to specimen geometry. The configurations finally

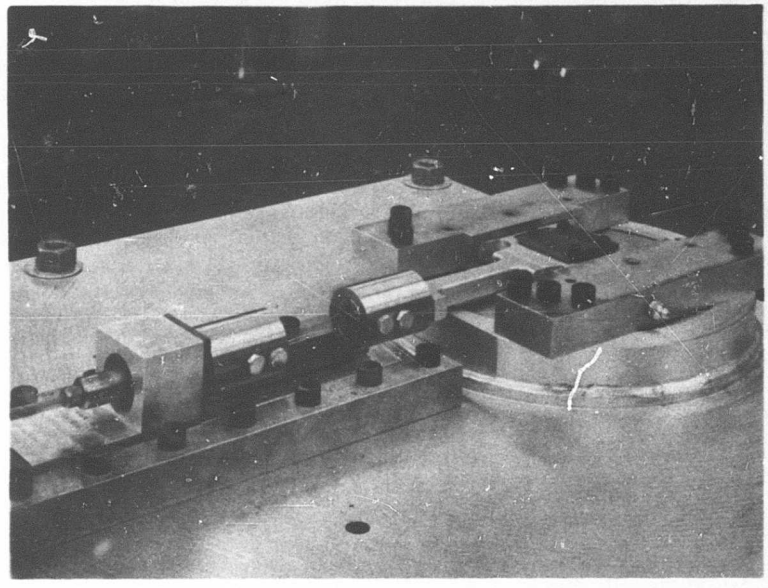

Figure 25. Cyclic Test Apparatus.

adopted were modifications of those employed by Baker, Mason, and Cratchley (Ref. 5). The new specimen configurations are shown in Figures 26 and 27. The wider specimens were used for cross-ply composites to increase the number of filament crossovers within the gage section. The use of these specimen configurations resulted in nearly complete elimination of specimen geometry- and grip-related failures.

A series of tests was performed using these specimen configurations. Glass-reinforced specimens with fiber orientations of 0°, 0°-90°, and $\pm 45^{\circ}$ were tested. Preload and machine displacement settings were sought which, at a rate of 40 cps, would result in fatigue failures in conveniently short times. Preload stress values adopted were about 1000 psi to 2000 psi, while the maximum stress ranged from 6000 psi to 18,500 psi (about 0.5 to 0.9 of the anticipated ultimate short-time strength of undamaged specimens). The load combinations employed gave R values (ratio of preload to maximum stress) between about 0.10 and about 0.15. The loads applied to the specimens were continuously monitored by feeding the load cell output into a high-speed oscillograph.

A detail of the fracture of a fatigued unidirectional glass-reinforced specimen is shown in Figure 28. This failure is entirely different from any observed in static testing. No stacked cracks are present, but there are arrays of fish-scale-like cracks emanating radially from broken fiber ends; and there are cracks parallel to, and between, fiber bundles. A definite boundary (arrow) is present between the region containing the fish-scale-like cracks and the uncracked region. Observation with polarized light revealed different refractive indices on each side of this boundary. This effect is often caused by excessive local heating and may be evidence that considerable heat was present at the time of fracture. There are also cracks close to the fibers, and running normal to the fibers, which do not extend into the region between bundles. These latter cracks are not easily discernible in Figure 28. Failure of this specimen occurred after 737 cycles. No load decay was evident before failure.

Figure 29 shows another unidirectional glass composite which failed after undergoing only 234 cycles. Although there was some evidence of heating, the effect was not nearly so pronounced as that shown in Figure 28. Larger cracks across the fiber bundles (arrows) extend into the matrix between the bundles. There was no load decay before failure. The difference between the two failure modes could be explained by a difference in temperature rise in the two specimens.

Cross-ply (0°-90°) specimens were tested: fracture occurred much more slowly, and was usually accompanied by several cycles of decreasing load. In Figure 30, a portion of a load-time oscillograph trace is reproduced which illustrates the load decay. The first cycle of decreased load is at A, and fracture occurred at B. Fatigue failure of all 0°-90° specimens was associated with transverse fiber bundles. A 0°-90° cross-ply specimen which fractured into three pieces (A, B, and C) is shown in Figure 31. Some stacked cracks accompanied this failure, although they are not nearly so closely spaced as those observed in the static test series.

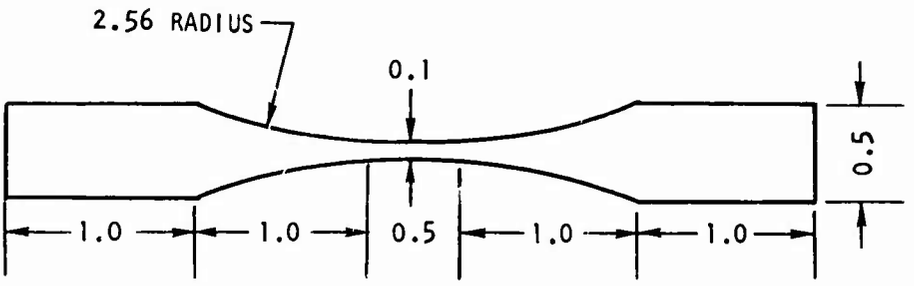

NOTE:ALL MEASUREMENTS IN INCHES

Figure 26. Unidirectional Composite Fatigue Specimen Configuration.

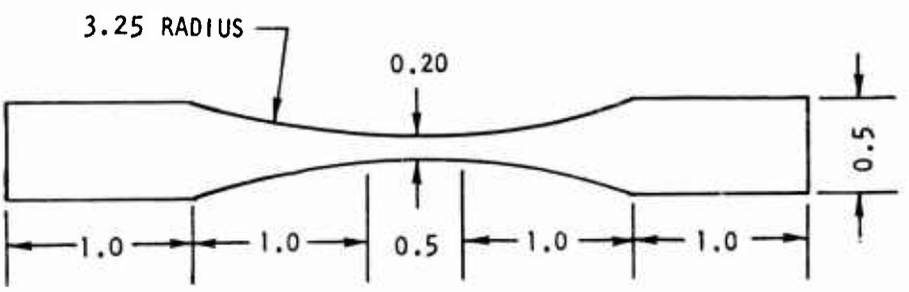

NOTE: ALL MEASUREMENTS IN INCHES

Figure 27. Cross-Ply Composite Fatigue Specimen Configuration.

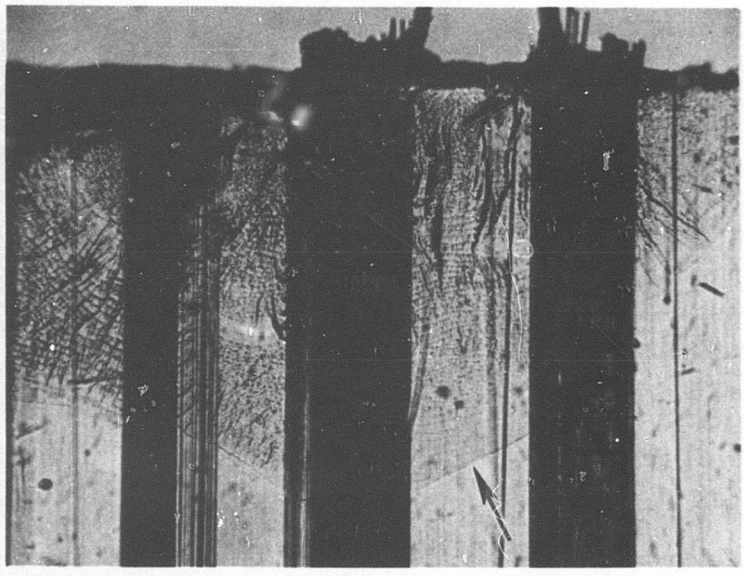

Figure 28. Detail of Fatigue Failure (after 737 cycles) of Unidirectional Glass-Reinforced Composite (50X).

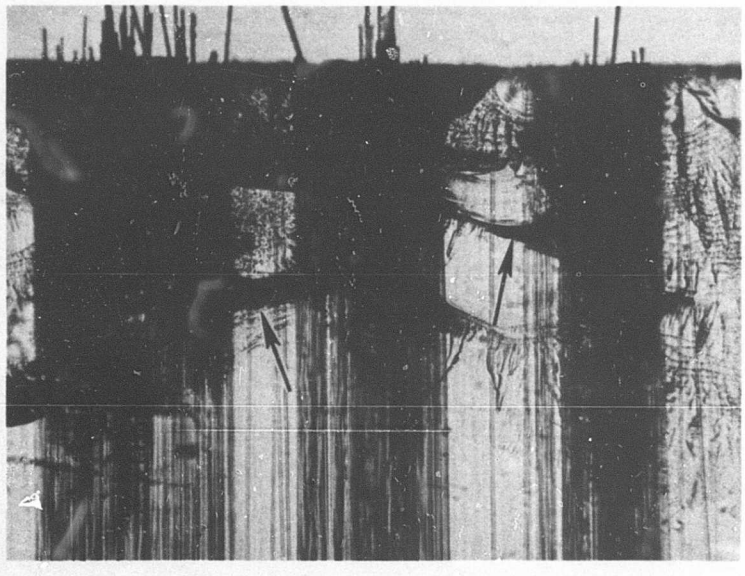

Figure 29. Detail of Fatigue Failure (after 234 cycles) of Unidirectional Glass-Reinforced Composite (50X).

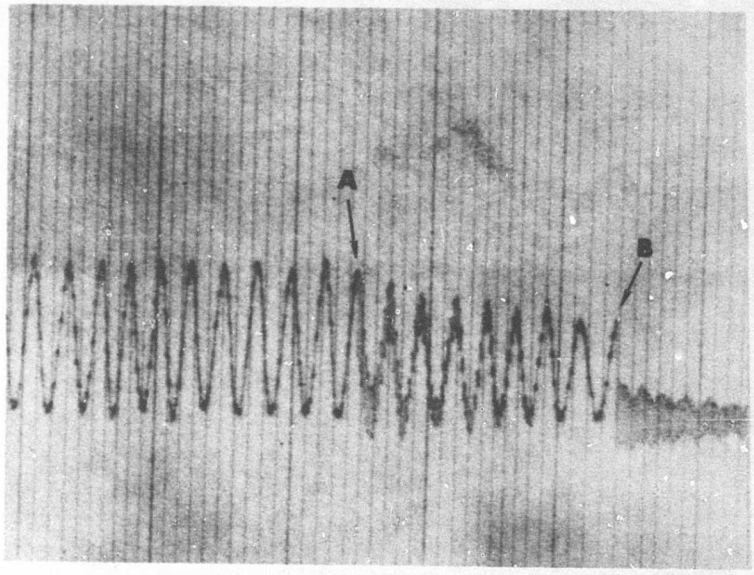

Figure 30. Portion of Load-Time Oscillograph Trace of 0°-90° Specimen Showing Load Decay Before Failure.

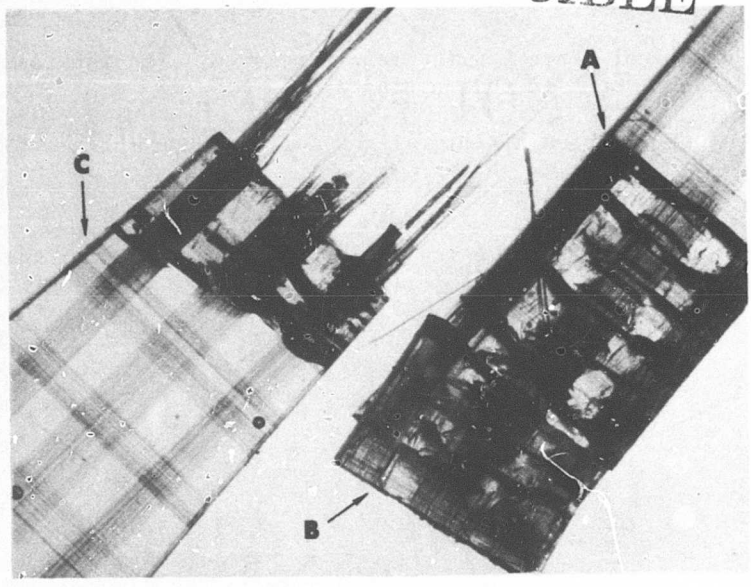

Figure 31. Fatigue Failure of Cross-Ply Glass-Reinforced Composite (12X).

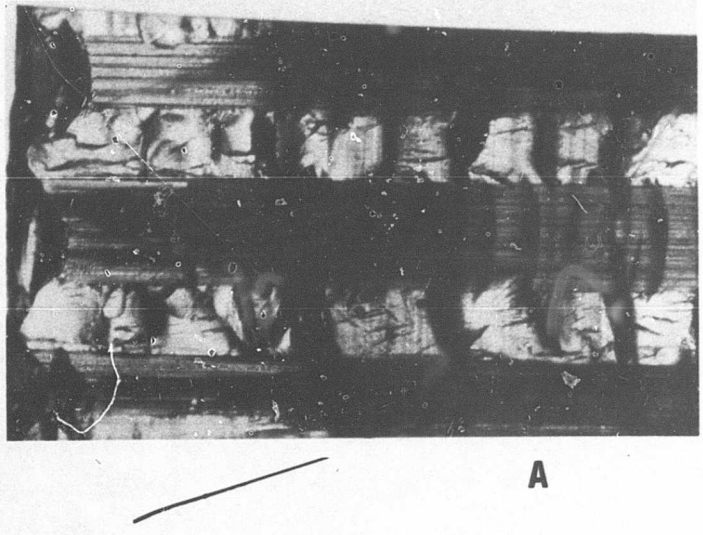

Figure 32. Detail of Fatigue Failure of Cross-Ply Glass-Reinforced Composite (23X).

Figure 32 is a detail of piece A with piece B removed. The interlaminar fracture surface can be seen in this photograph.

A shear mechanism was the predominant fatigue failure mode in the $\pm 45^{\circ}$ cross-ply specimens. The fracture surface always passed through the fiber bundles. No load decay was observed with the $\pm 45^{\circ}$ specimens.

A plot of maximum tensile stress versus cycles to failure for all the specimens tested is presented in Figure 33. The curve for the 0° specimens is a straight line from 1 cycle to 30,000 cycles. The curves for the 0°-90° and $\pm 45^{\circ}$ specimens appear bilinear over this range. Each of these curves is essentially horizontal from 1 cycle to approximately 500 cycles. The slopes for all three curves from 500 to 30,000 cycles are approximately the same.

The presence of voids and damaged fibers had a considerable effect on the cycle life of 0° fiberglass-reinforced specimens. In each case, failure occurred through the regions containing the flaws. No weakening effect was noted when one specimen containing fibers contaminated with mold release was tested. Although fracture passed through the contaminated region, the data point falls on the upper limit of the scatter band in Figure 33.

A reduction of cycle life was also experienced by the 0°-90° fiberglass specimens when voids or cut filaments were introduced. Specimens of $\pm 45^{\circ}$ orientation with preexisting flaws were not tested.

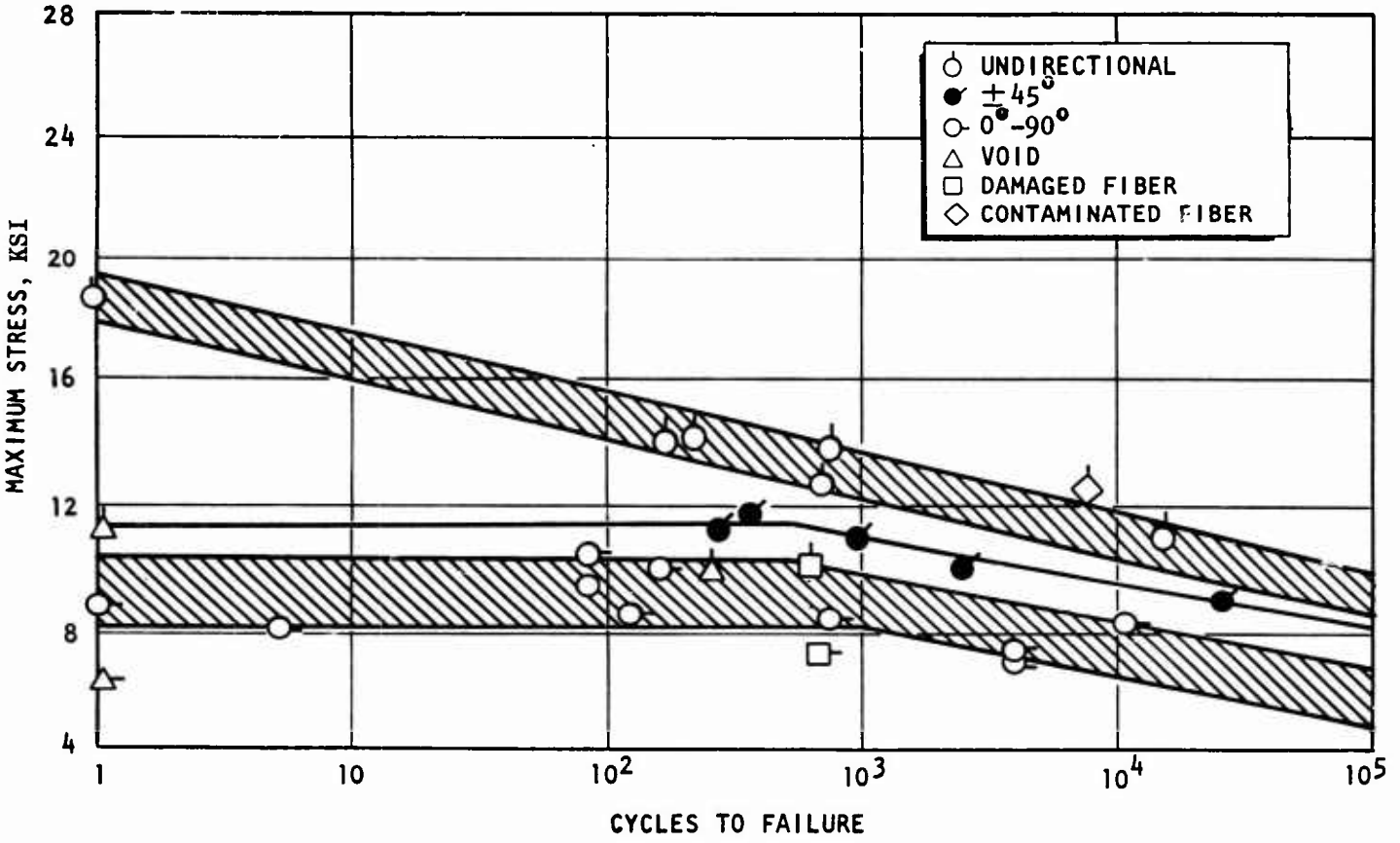

Figure 33. Cyclic Fatigue for Glass PL-1 Composites.

IMPACT TESTING

An exploratory test series was undertaken to reveal pertinent aspects of crack propagation in reinforced composites as a result of impulsive loading. A pendulum-type apparatus was assembled for impulse loading of reinforced specimens. This apparatus, shown in Figure 34, consists of a pendulum with variable weights, a specimen holder, and a protractor to measure the initial angular displacement of the pendulum. The specimens were flat plates with dimensions of 1.1 inches by 1.1 inches by 0.09 inch. The impulsive load was applied to the edge of the specimen.

An unreinforced specimen was tested for comparison with subsequently tested reinforced specimens. Upon impact, a single crack propagated from the region of impact in a helical configuration. The crack made an angle of approximately 30° with the direction of impact. A low-order residual stress field was evident in the vicinity of the crack. Severe stresses were observed in the impact region due to local crushing of the plastic.

All the reinforced plates tested exhibited greater impact resistance than the unreinforced plate from the standpoint of length of crack propagation and amount of energy to propagate a crack. In most cases, considerable difficulty was encountered in achieving internal failure of reinforced specimens without causing complete destruction. Part of this difficulty may have been caused by a small misalignment between the striking head and specimen, or by play in the pendulum pivot point. These effects would be accentuated at the higher input energy levels required for crack propagation in the reinforced plates.

It was observed in 0°-90° Morganite specimens that it was more difficult to propagate a crack when a 90° fiber bundle was at the surface than when impact was on a matrix-rich region. Further, the propagating crack made an angle of approximately 45° to the impact direction (compared to 30° in the unreinforced plate). For a 0°-90° fiberglass specimen, a propagating crack tended to follow fairly closely the angle observed in the unreinforced plate.

The trend of impulsively created cracks in fiberglass-reinforced specimens to follow the angle for an unreinforced plate (30°), and of Morganite-reinforced plates to exhibit a different angle of propagation (45°), persisted with 0° specimens. Although it was not possible to pursue this point, it may prove to be a significant characteristic of impact response of reinforced composites. One major difference was observed between the 0° and 0°-90° specimens. Each of the 0° specimens tended to delaminate at the region of impact. This was not evident with the 0°-90° specimens.

High-speed photographic techniques were employed to stop the crack propagation action. A Milliken camera operating at 400 frames per second was found to be too slow; consequently, a Fastax camera operating at 3000 frames per second was employed. However, the tests performed with Fastax coverage did

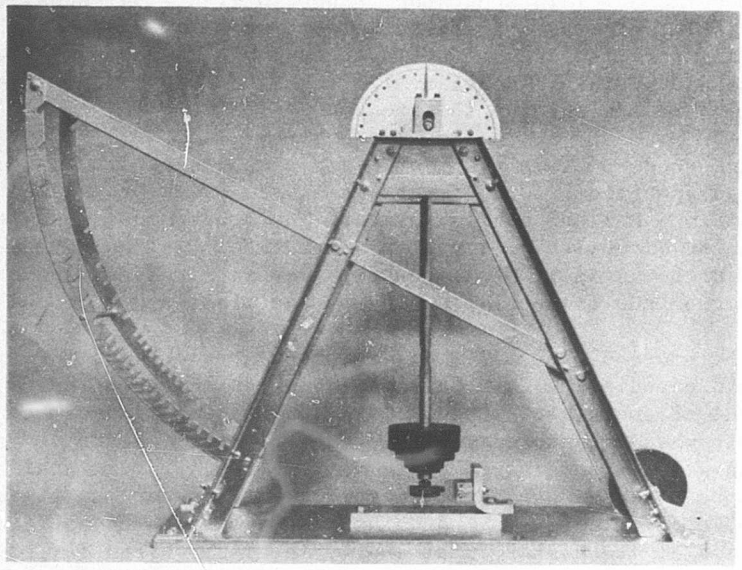

Figure 34. Impact Test Apparatus.

not achieve any internal fractures. Selected frames from one of these tests are presented in Figure 35. These show the progression of symmetrical strain patterns through the material from the point of impact. The occasional occurrence of an indistinct pattern (e.g., second from left in Figure 35) was repeated at irregular intervals over the entire film clip; a possible explanation is interference from reflected waves.

Detailed examination of some of the patterns in a 0°-90° Morganite-reinforced specimen disclosed discontinuities in strain caused by the fibers. It is possible that further work may establish a correlation between this phenomenon and the characteristic fracture angle in the graphite-fiber-reinforced material.

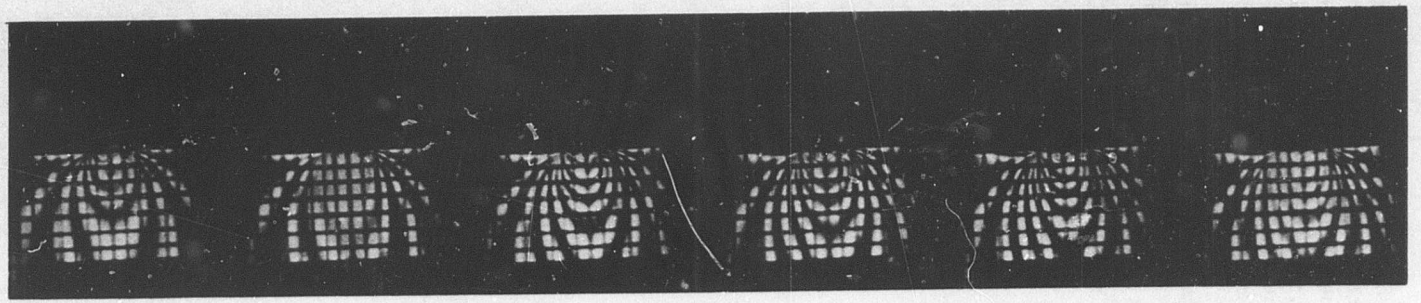

(a) (b) (c) (d) (e) (f)

Figure 35. Propagation of Strain Waves in 0°-90° Fiberglass-Reinforced Plate After Impact (frames at 3000/sec, commencing 0.003 second after impact) (1.0X).

SUMMARY OF RESULTS

A wide variety of observations has been made concerning crack initiation and propagation in fiber-reinforced composites. The techniques of photoelasticity have proven to be useful in relating flaws to ultimate failure of composites. It was not feasible to complete an entire test matrix including both fiberglass and Morganite graphite fiber, the three fiber orientations of interest (0°, 0°-90°, and $\pm 45^\circ$), and uniaxial and biaxial, static and dynamic testing. However, some direct comparisons can be made. The results of these investigations can be summarized as follows:

UNIAXIAL TENSION TESTS

1. Failure of 0° fiberglass-reinforced specimens was a brittle-type fracture accompanied by unbonding of fiber bundles away from the crack surface. Distinct residual stress patterns were present after fracture.
2. Fracture of 0°-90° fiberglass specimens initiated at a transverse fiber bundle and was accompanied by arrays of stacked, dish-shaped cracks concave toward the fracture surface. Unbonding of fiber bundles propagated away from the fracture. Transverse fiber bundles tended to inhibit propagation of unbonding and to confine stacked crack arrays.
3. Specimens with $\pm 45^\circ$ fiber orientation failed in a shear mode along the fibers. Failure always initiated at fiber crossover points located at or near edges of the specimen. Some local stacked cracks formed at fiber crossover points.
4. Difficulty was encountered in wetting the Morganite fibers with the photoelastic matrix material. This difficulty was not present with fiberglass. Precise comparison of composites made from graphite and from glass fibers was generally not possible.
5. Failure of 0° Morganite-reinforced specimens was of a brittle type. Some small secondary cracks were seen near the main crack. No unbonding propagated away from the main crack, as was the case with fiberglass. With these specimens there was a rather uniform, low-order residual stress field. In some specimens, unbonding preceded ultimate failure. This unbonding occurred incrementally over most of the specimen before failure occurred. Examination of bonded regions revealed microscopic matrix cracks normal to the fiber. These were residual stresses associated with the unbonding in these specimens.
6. Initiation of failure in 0°-90° Morganite specimens was similar to that in the fiberglass specimens: fracture always started at a transverse fiber bundle. However, there were no stacked crack arrays and no unbonding in the 0°-90° Morganite specimens.

7. Small voids in 0° fiberglass-reinforced specimens had no apparent effect on failure mode. Large voids reduced the strength of 0° specimens and altered the nature of fracture. When large voids were present, stacked cracks formed. Unbonding also propagated away from the main crack.

8. Damaged filaments in 0° fiberglass specimens tended to decrease the strength and to result in a brittle-type failure through the damaged filament region. No stacked crack arrays were evident.

9. Specimens containing fiber bundles contaminated with mold release did not deviate significantly from the failure pattern or ultimate stress observed in specimens with uncontaminated glass fibers.

10. Initial flaws did not have a great effect on 0°-90° fiberglass specimens. The dominating factor of failure was always the transverse fiber bundles.

11. Fiberglass-reinforced specimens in $\pm 45^{\circ}$ orientation exhibited extreme sensitivity to the presence of voids. Failure was a shear type passing through the voids. Local stacked cracks occurred at crossover points, and there was some fiber unbonding away from the crossover points.

12. Damaged Morganite fiber bundles in 0° specimens reduced the load-carrying capacity. Fracture occurred through the damaged fiber region.

BIAXIAL TESTS

1. Compression-tension biaxial stress fields, obtained from diametral compression disks, resulted in different fracture modes from those observed in uniaxial tests. No stacked cracks were observed. However, a crazing phenomenon occurred which was never present in uniaxial tests. The occurrence of crazing did not constitute failure, although the rate of load increase tended to decrease at constant crosshead rate. Crazing occurred near the center in all 0° and 0°-90° fiberglass and in the 0° Morganite disks. The craze marks in the Morganite disks were much finer than those observed in the fiberglass disks. In all cases the crazing displayed a strong tendency to be confined by adjacent fiber bundles.

   Fracture in the 0° fiberglass and Morganite disks occurred through vertical fiber bundles. The 0° Morganite specimens exhibited unbonding, starting at a central fiber bundle and then occurring at adjacent fiber bundles.

   In the 0°-90° Morganite specimen, fracture did not pass through a vertical fiber bundle. A vertical crack propagated across several horizontal fiber bundles, resulting in fiber unbonding and pullout near the crack. There is some indication that the unbonding preceded, and probably caused, the fracture.

2. Several attempts to achieve failure in a tension-tension biaxial strip test were unsuccessful. However, some aspects of crack propagation in a tensile field were observed. In a 0°-90° fiberglass plate, fracture tended to follow a path parallel to the horizontal fibers (i.e., perpendicular to the applied tensile load axis). Some stacked cracks and unbonding were associated with the propagating crack. Failure of a 0° plate revealed bifurcations of propagating cracks. This aspect of crack propagation should be included in subsequent analytical treatments.

   Propagating cracks in a $\pm 45^{\circ}$ plate almost invariably passed through fiber bundle crossover points. Crack bifurcations were again present.

CYCLIC TESTS

1. A cyclic load apparatus was designed and fabricated for low-cycle fatigue studies. Specimen configurations and serrated end grips were adopted and resulted in a very low incidence of grip-related failures.
2. Failure modes for 0° glass specimens included the formation of arrays of fish-scale-type cracks in the vicinity of the fracture surface. Some evidence of localized heating was observed. Fracture was always very rapid, and there was no observable load decay before failure.

   The 0°-90° fiberglass-reinforced specimens usually exhibited several cycles of load decay before failure. There were some stacked crack formations, but they were not so closely spaced as those observed in the static test series.

   Failure of the $\pm 45^{\circ}$ specimens was a shear-type fracture along the fiber bundles. No load decay was observed before fracture.
3. The curve of maximum stress versus cycles to failure for the 0° specimens was linear in the range from 1 cycle to 30,000 cycles. The curves for the 0°-90° and $\pm 45^{\circ}$ specimens were bilinear over this range.
4. Voids and damaged fibers reduced the cycle life of 0° and 0°-90° fiberglass-reinforced specimens. Fracture occurred through the regions containing flaws. Contamination of fibers in a 0° specimen resulted in no decrease in cycle life. Fracture did pass through the contaminated region. Flawed $\pm 45^{\circ}$ specimens were not tested.

IMPACT TESTS

1. The presence of reinforcing elements in a plastic matrix increased impact resistance.
2. Different angles of propagation of an impact-produced crack were observed between the fiberglass and the Morganite plates. Direction of crack propagation of a fiberglass-reinforced specimen was similar to that of an unreinforced plate.

CONCLUSIONS

1. The use of photoelastic models of composite materials for kinematic studies of fracture mode and fracture propagation is feasible and produces meaningful information. The present work showed that cross-ply configurations yield particularly important data, as functions of fiber identity, orientation, and manner of mechanical loading, as well as of the presence of artificially introduced flaws.

2. The significance of photoelastic observations was greatly increased by making concurrent load-deflection recordings. Further advances are possible through quantitative descriptions of crack propagation and their correlation with such other quantities as energy absorption data.

3. The microphotoelastic techniques used, ranging from "stills" to Fastax camera operation at several thousand frames per second, adequately covered most of the fracture propagation processes of interest. Further advances in high-speed techniques are possible through use of a camera-triggering device actuated, for example, by changes in loading rate in tensile testing, by changes in maximum load in cyclic fatigue, and by pendulum position in impacting. "Stop-action" photography might be facilitated in the impact case by use of a Kerr cell, but the need for this was not established by the present work. Predicting both the location and the instant of brittle fracture of 0° fibers in simple tension is a major difficulty which argues against an attempt to improve high-speed techniques in that one case.

4. The role of the matrix in distributing the load among fibers was clearly evidenced by the present work, as was also the importance of the fiber-matrix interfacial bond in implementing that role. There is some evidence that the characteristics of the failed composite in the vicinity of a fracture (e.g., the pattern of stacked, dish-shaped cracks along a single 0° fiber) are related to the interfacial bond quality.

5. Failure modes in simple tension, in biaxial compression-tension and tension-tension, and in cyclic fatigue all indicated that fibers oriented at angles to the principal tensile stress constitute flaws in the mechanical system on which failure initiates and propagates. The fiber-matrix interfacial bond played a major role in these failures, as illustrated by the characterisitc shear mode in $\pm 45^{\circ}$ cross-ply configurations and the characteristic parting along 90° fibers in simple tension.

6. Edge effects (i.e., fiber emergences nonparallel to the tensile axis) were particularly prominent. The potential utility of photoelastic failure investigation as a means of evaluating and developing joining and load-transmission configurations for composites is obvious. The comparison of heat-aged with as-fabricated composites is also suggested, to

attempt to determine whether failures in the former are induced by thermo-oxidative changes in the matrix bulk properties, or by diminished interfacial bond strength, or (in the latter case) by exaggerated weakening at fiber emergences as compared with the interior. These distinctions could be made by observing detailed differences in the fracture characteristics.

7. Cut fibers in 0^{o} orientation affected strength and failure mode more dramatically than did the introduction of isolated matrix flaws or unbonded regions. On the other hand, the latter types of flaws also had dramatic effects when the fibers were in shear orientations to the load axis. These observations are in good accord with those of 4 and 5 above.

8. Detailed differences in failure patterns observed under different combinations of fiber identity, orientation, loading rate, and biaxiality ratio require further study. Some examples are the stacked cracks, crazing, crack bifurcation, and fiber unbonding. Interpretation of such observations must take into account the nature of the model specimen (e.g., fiber spacing, overall fiber density, bonding peculiarities of the PL-1/Morganite system, etc.). Additional developments in these areas can lead to still further specific descriptions of optimum design features of multilaminates.

9. It may be possible, after further study, to exploit certain failure modes observed in these investigations to provide an alternative to the commonly used interlaminar beam shear test. For example, it may be possible to use the formation of stacked, dish-shaped cracks as an index of interfacial bond quality. Utilization of the shear mode failure in a tensile bar containing one or more parallel fibers oriented at some angle to the load axis might also provide an alternative to the standard interlaminar shear test.

RECOMMENDATIONS

The current investigations have indicated many aspects of reinforced composite fracture that should be studied further. Among these are:

UNIAXIAL TESTS

1. Perform further studies on the significance of the formation of stacked crack arrays, particularly with reference to interfacial bonding.

2. Investigate further the effects of flaws in compression and shear stress fields, both with respect to composite design and as a means of evaluating interfacial bonding.

3. Investigate load concentration and fracture in specimens having notches, cutouts, holes, and other edge configurations specifically related to joining and load-transmission, as well as to heat-aging phenomena.

4. Conduct further tests to establish criteria and characteristics of crack bifurcation and other failure patterns related to specific combinations of material and load.

CYCLIC TESTS

1. Perform cyclic tensile fatigue tests on graphite-reinforced composites.

2. Pursue relationships between cyclic tensile and compressive load, frequency, lifetime, load decay before fracture, fracture mode, and reinforcement and matrix characteristics (fiber type, orientation, interfacial bond, matrix heating, embrittlement, etc.).

3. Perform flexural fatigue tests similar to 1 above.

4. Evaluate fatigue effects on specimens having notches, cutouts, etc., relative to load concentration and to the susceptibility of edge configurations to early failure initiation.

IMPACT TESTS

1. Repeat present tests with improved photographic techniques (especially Fastax triggering).

2. Perform simple flexural impact tests (i.e., center of clamped disk).

3. Impact specimens containing cutouts (notches, holes, slots).

MATERIAL MODELING

1. Improve means of isolating, coating, and embedding of graphite fibers.

2. Increase the number of plies in cross-ply configurations.

3. Increase the density of reinforcing fibers or bundles in each ply.

REFERENCES

1. Bouc, C. A.: Microscopic Study of Mode of Fracture in Filament-Wound Glass Resin Composites, TAM Report No. 234, Department of Theoretical and Applied Mechanics, University of Illinois, November 1962

2. Mullin, J., J. M. Berry, and A. Gatti: "Some Fundamental Fracture Mechanisms Applicable to Advanced Filament Reinforced Composites," J. Composite Materials, Vol. 2, No. 1, January 1968.

3. Hetenyi, M.,Editor: Handbook of Experimental Stress Analysis, J. Wiley and Sons, Inc., New York, 1950.

4. Smith, E. J.: "Crack Bifurcation in Brittle Solids," J. Mech. Phys. Solids, Vol. 16, pp 329-336, September 1968.

5. Baker, A. A., J. E. Mason, and D. Cratchley: "High-Strain Fatigue Studies of a Composite Material," J. Materials Science, Vol. 1, No. 3, August 1966.

Unclassified
Security Classification

DOCUMENT CONTROL DATA - R & D

(Security classification of title, body of abstract and indexing annotation must be entered when the overall report is classified)

1. ORIGINATING ACTIVITY (Corporate author) Rocketdyne a Division of North American Rockwell Corporation Canoga Park, California	2a. REPORT SECURITY CLASSIFICATION Unclassified 2b. GROUP

3. REPORT TITLE

FLAW POINT AND DYNAMIC MICROPHOTOELASTICITY INVESTIGATION

4. DESCRIPTIVE NOTES (Type of report and inclusive dates)

Final Report, 24 January 1968 to 19 February 1969

5. AUTHOR(S) (First name, middle initial, last name)

Angelo A. Caputo
John E. Hilzinger

6. REPORT DATE	7a. TOTAL NO. OF PAGES	7b. NO. OF REFS
June 1969	64	5

8a. CONTRACT OR GRANT NO.	9a. ORIGINATOR'S REPORT NUMBER(S)
DAAJ02-68-C-0023 b. PROJECT NO. Task 1F162204A17002 c. d.	USAAVLABS Technical Report 69-42 9b. OTHER REPORT NO(S) (Any other numbers that may be assigned this report)

10. DISTRIBUTION STATEMENT

This document is subject to special export controls and each transmittal to foreign governments or foreign nationals may be made only with prior approval of US Army Aviation Materiel Laboratories. Fort Eustis, Virginia 23604.

11. SUPPLEMENTARY NOTES	12. SPONSORING MILITARY ACTIVITY
	US Army Aviation Materiel Laboratories Fort Eustis, Virginia

13. ABSTRACT

The effects of load-induced flaws and preexisting flaws on the initiation and propagation of fracture in glass- and graphite-fiber-reinforced composites were studied, utilizing a birefringent epoxy resin matrix with relatively wide-spaced unidirectional and simple ~~(0°-90° and ±45°)~~ cross-ply fiber configurations, and combining photoelastic and high-speed photographic techniques. A broad, qualitative investigation was made to characterize differences in behavior as functions of ply type and orientation, fiber identity, type of flaw (exposed edges, interior bubbles, cut filaments, and unbonded fibers), and manner of loading. Specimens were examined under simple static tension, biaxial static compression-tension and tension-tension, cyclic tension, and dynamic impact, in all cases at room temperature.

Fractures were often initiated by or drawn into the identified flaws; and fibers at angles to the principal tensile axis also constituted weak structural elements. Reduction of strength or cycle life often resulted from introduction of flaws. Fracture mode tended toward brittle in unidirectional (0^0) composites and toward more complex tearing and shearing processes in other configurations and under complex loading. Formation of stacked cracks or crazing in the resin, progressive fiber unbonding, and crack bifurcation were other details observed under specific combinations of material and test parameters.

DD FORM 1 NOV 68 1473 REPLACES DD FORM 1473, 1 JAN 64, WHICH IS OBSOLETE FOR ARMY USE.

Unclassified
Security Classification

14. KEY WORDS	LINK A		LINK B		LINK C	
	ROLE	WT	ROLE	WT	ROLE	WT
Composites						
Failure of Composites						
Flaws in Composites						
Fracture of Composites						
Glass Fiber Reinforced Composites						
Graphite Fiber Reinforced Composites						
Mechanical Properties of Composites						
Micromechanics of Composites						
Photoelastic Study of Composites						